JHEP03 (2017) 162

Search for massive resonances decaying into WW, WZ or ZZ bosons in proton-proton collisions at $\sqrt{s} = 13$ TeV

The CMS collaboration

E-mail: cms-publication-committee-chair@cern.ch

ABSTRACT: A search is presented for new massive resonances decaying to WW, WZ or ZZ bosons in $\ell\nu q\bar{q}$ and $q\bar{q}q\bar{q}$ final states. Results are based on data corresponding to an integrated luminosity of 2.3–2.7 fb^{-1} recorded in proton-proton collisions at $\sqrt{s} = 13$ TeV with the CMS detector at the LHC. Decays of spin-1 and spin-2 resonances into two vector bosons are sought in the mass range 0.6–4.0 TeV. No significant excess over the standard model background is observed. Combining the results of the $\ell\nu q\bar{q}$ and $q\bar{q}q\bar{q}$ final states, cross section and mass exclusion limits are set for models that predict heavy spin-1 and spin-2 resonances. This is the first search for a narrow-width spin-2 resonance at $\sqrt{s} = 13$ TeV.

Contents

1 Introduction

Several theories beyond the standard model (SM) predict the existence of heavy particles that preferentially decay to pairs of vector bosons V, where V represents a W or Z. These models usually aim to clarify open questions in the SM such as the apparently large difference between the electroweak and the gravitational scales. Notable examples of such models include the bulk scenario [1–3] of the Randall-Sundrum warped extra-dimensions (RS1) [4, 5] and a heavy vector-triplet (HVT) model [6]. The bulk graviton model is described by two free parameters: the mass of the first Kaluza-Klein (KK) excitation of a spin-2 boson (the KK bulk graviton G_{bulk}) and the ratio $\tilde{k} \equiv k/\overline{M}_{Pl}$, where k is the unknown curvature scale of the extra dimension and $\overline{M}_{Pl} \equiv M_{Pl}/\sqrt{8\pi}$ is the reduced Planck mass. The HVT generalises a large number of models that predict spin-1 charged (W′) and neutral (Z′) resonances. Such models can be described in terms of just a few parameters: two coefficients c_F and c_H, scaling the couplings to fermions, and to the Higgs and longitudinally polarized SM vector bosons respectively, and the strength g_V of the new vector boson interaction. Two benchmark models are considered in the HVT scenario. In the first one, referred to as HVT model A, with $g_V = 1$, weakly coupled vector resonances arise from extensions of the SM gauge group, such as the sequential standard model (SSM) [7], that have comparable branching fractions to fermions and gauge bosons. In HVT Model B with $g_V = 3$, the new resonances have large branching fractions to pairs of bosons, while their fermionic couplings are suppressed. This scenario is most representative of composite models of Higgs bosons.

Searches for diboson resonances have been previously performed in many different final states, placing lower limits on the masses of these resonances above the TeV scale [8–19]. Searches performed with proton-proton collisions at $\sqrt{s} = 8$ TeV indicated deviations from background expectations at resonance masses of about 2 TeV. The largest excesses of events were observed in the searches in the dijet WW, WZ or ZZ [12, 16] channels, as well as in the semi-leptonic WH → $\ell\nu b\overline{b}$ final state [13], and have local significances of 3.4σ and 2.2σ, respectively. The most stringent lower mass limit for a W′ (Z′) is set at 2.3 (2.0) TeV by a combination of searches in semi-leptonic and all-hadronic final states performed with proton-proton collisions at $\sqrt{s} = 13$ TeV [9]. The same searches provide the current lower mass limit of 2.6 TeV for a HVT.

This paper presents a search for resonances with masses above 0.6 TeV decaying into a pair of vector bosons. The analysis is based on data collected in proton-proton collisions at $\sqrt{s} = 13$ TeV with the CMS experiment at the CERN LHC during 2015, corresponding to an integrated luminosity of 2.3 and 2.7 fb^{-1} for the $\ell\nu q\overline{q}$, where $\ell = \mu$ or e, and $q\overline{q}q\overline{q}$ final state, respectively. The $\ell\nu$+jet search also includes the W → $\tau\nu$ contribution from the decay $\tau \to \ell\nu\overline{\nu}$. The gain in sensitivity from τ leptons is limited by the small branching fractions involved.

The key challenge of the analyses is the reconstruction of the highly energetic decay products. Since the resonances under study have masses of order 1 TeV, their decay products, i.e. the bosons, have on average transverse momenta (p_T) of several hundred GeV or more. As a consequence, the particles emerging from the boson decays are very collimated.

In particular, the jet-decay products of the bosons cannot be resolved using the standard algorithms, but are instead reconstructed as a single jet object. Dedicated techniques, called jet "V tagging" techniques, are applied to exploit the substructure of such objects, to help resolve jet decays of massive bosons [20, 21]. The V tagging also helps suppress SM backgrounds, which mainly originate from the production of multijet, W+jets, and nonresonant VV events.

The final states considered are either $\ell\nu q\overline{q}$ or $q\overline{q}q\overline{q}$, where the hadronic decay products of the V decay are reconstructed in a single jet. They result in events with either a charged lepton, a neutrino, and a single reconstructed jet ($\ell\nu$+jet channel), or two reconstructed jets (dijet channel). As in the analyses of previous data [11, 12], the aim is to reconstruct all decay products of the new resonance to be able to search for a localized enhancement in the diboson invariant mass spectrum. While the analyses in general aim at large resonance masses, we conduct two exclusive searches in the $\ell\nu$+jet final state, separately optimized for the mass ranges 0.6–1.0 TeV ("low-mass") and > 1 TeV ("high-mass").

This paper is organized as follows. Section 2 briefly describes the CMS detector. Section 3 gives an overview of the simulations used in this analysis. Section 4 provides a detailed description of the reconstruction and event selection. Section 5 describes the background estimation and the signal modelling procedures. Systematic uncertainties are discussed in section 6. The results of the search for a spin-2 bulk graviton and for spin-1 resonances as predicted by HVT models are presented in section 7, and section 8 provides a brief summary.

2 The CMS detector

The central feature of the CMS apparatus is a superconducting solenoid of 6 m internal diameter, providing a magnetic field of 3.8 T. Contained within the solenoid volume are a silicon pixel and strip tracker, a lead tungstate crystal electromagnetic calorimeter (ECAL), and a brass and scintillator hadron calorimeter (HCAL), each composed of a barrel and two endcap sections. Extensive forward calorimetry complements the coverage provided by the barrel and endcap detectors. The forward hadron (HF) calorimeter uses steel as an absorber and quartz fibers as the sensitive material. The two halves of the HF are located 11.2 m from the interaction region, one on each end, and together they provide coverage in the pseudorapidity range $3.0 < |\eta| < 5.2$. Muons are measured in gas-ionization detectors embedded in the steel flux-return yoke outside the solenoid.

A particle-flow (PF) event algorithm [22, 23] reconstructs and identifies each individual particle with an optimized combination of information from the various elements of the CMS detector. The energy of photons is obtained from the ECAL measurement, corrected for suppression of small readout signals. The energy of electrons is determined from a combination of the electron momentum at the primary interaction vertex as determined by the tracker, the energy of the corresponding ECAL cluster, and the energy sum of all bremsstrahlung photons spatially compatible with originating from the electron track. The momentum of muons is obtained from the curvature of the corresponding track. The energy of charged hadrons is determined from a combination of their momentum measured in the tracker and the matching of energies deposited in ECAL and HCAL, also corrected for

suppression of small signals and for the response function of the calorimeters to hadronic showers. Finally, the energy of neutral hadrons is obtained from the corresponding corrected ECAL and HCAL energy.

A more detailed description of the CMS detector, together with a definition of the coordinate system and the kinematic variables, can be found in ref. [24].

3 Simulated samples

The bulk graviton model and HVT models are used as benchmark signal processes. In these models, the vector gauge bosons are produced with a longitudinal polarization in more than 99% of the cases. For each resonance hypothesis, we consider masses in the range 0.6 to 4.0 TeV. Simulated signal events are generated at leading order (LO) accuracy with MADGRAPH5_aMC@NLO v2.2.2 [25] with a width of 0.1% of the resonance mass.

The Monte Carlo (MC) generated samples of SM backgrounds are used to optimize the analyses. The W+jets SM process is simulated with MADGRAPH5_aMC@NLO, while $t\bar{t}$ and single top quark events are generated with both POWHEG v2 [26–31] and MAD-GRAPH5_aMC@NLO. Diboson (WW, WZ, and ZZ) processes are generated with PYTHIA v8.205 [32, 33]. Parton showering and hadronization are implemented through PYTHIA using the CUETP8M1 tune [34, 35]. The NNPDF 3.0 [36] parton distribution functions (PDFs) are used for all simulated samples, except for diboson ones (WW, WZ and ZZ) for which NNPDF 2.3LO is used. All events are processed through a GEANT4-based [37] simulation of the CMS detector. The simulated background is normalized using inclusive cross sections calculated at next-to-leading order (NLO), or next-to-NLO order in quantum chromodynamics (QCD) where available, using MCFM v6.6 [38–41] and FEWZ v3.1 [42].

Additional simulated minimum-bias interactions are added to the generated events to match the additional particle production observed in the large number of overlapping proton-proton interactions within the same or nearby bunch crossings (pileup). The simulated events are corrected for differences between data and simulation in the efficiencies of the lepton trigger [43], lepton identification and isolation [43], and selection of jets originating from hadronization of b quarks (b jets) [44].

4 Reconstruction and selection of events

4.1 Trigger and preliminary offline selection

In the $\ell\nu$+jet channel, events are collected with a trigger requiring either one muon or one electron. For the low-mass $\ell\nu$+jet analysis, both triggers have a p_T requirement of 27 GeV. The muons and electrons selected online also satisfy both isolation requirements and identification criteria. The selection efficiency of these triggers for leptons satisfying the offline requirements described in section 4.3, varies in the range 90–95% for the single-muon trigger, depending on the η of the muon, and it is >94% for the single-electron trigger. In the high-mass $\ell\nu$+jet analysis, muons selected online must have $p_T > 45$ GeV and $|\eta| < 2.1$, while the minimum p_T threshold for electrons is 105 GeV. There are no requirements on the isolation and loose identification criteria are used, since these introduce inefficiencies at high resonance masses. The selection efficiencies with respect to the offline requirements

of the single-muon trigger vary between 90% and 95%. The efficiency is above 98% for the single-electron trigger.

In the dijet channel, events are selected online using a variety of different hadronic triggers based on the scalar p_T sum of all jets in the event (H_T) or the presence of at least one jet with loose substructure requirements; the details of jet substructure are described in section 4.4. Events must satisfy at least one of the following four requirements. The first requirement is simply $H_T > 800\,\text{GeV}$. The second requirement is $H_T > 650\,\text{GeV}$ and a difference in η between the two leading jets in the event satisfying the condition $\Delta\eta < 1.5$. The accepted jets are further required to have a dijet invariant mass $> 900\,\text{GeV}$. The third criterion is that at least one jet with $p_T > 360\,\text{GeV}$ and a trimmed mass (as defined in section 4.4) $m_{\text{jet}} > 30\,\text{GeV}$ is present in the event. Fourthly, events with $H_T > 700\,\text{GeV}$ and at least one jet with $m_{\text{jet}} > 50\,\text{GeV}$ are also selected for analysis.

The pp data collected by CMS with the detector in its fully operational state correspond to $2.3\,\text{fb}^{-1}$ of integrated luminosity [45]. Additional data equivalent of $0.37\,\text{fb}^{-1}$ of integrated luminosity were collected with the HF running in suboptimal conditions; those data are used only for the dijet channel, since jets reconstructed online and used for the calculation of H_T are in the range of $|\eta| < 3.0$. The trigger efficiency is found to be unaffected by the condition of the HF.

Offline, all events are required to have at least one primary interaction vertex reconstructed within a 24 cm window along the beam axis, with a transverse distance from the mean pp interaction point of less than 2 cm [46]. In the presence of more than one vertex passing these requirements, the primary interaction vertex is chosen to be the one with the highest total p_T^2, summed over all the associated tracks.

4.2 Jet reconstruction

Jets are clustered from the four-momenta of the particles reconstructed using the CMS PF algorithm, from the FASTJET software package [47]. In the jet clustering procedure charged PF candidates not associated with the primary interaction vertex are excluded. Jets used for identifying the W and Z boson decays to $q\bar{q}$ are clustered using the anti-k_T algorithm [48] with distance parameter $R = 0.8$ ("AK8 jets"). To identify b jets, the anti-k_T jet clustering algorithm is used with $R = 0.4$ ("AK4 jets"), along with the inclusive combined secondary vertex b tagging algorithm [44, 49]. The chosen algorithm working point provides a misidentification rate of $\approx 1\%$ and efficiency of $\approx 70\%$. A correction based on the area of the jet projected on the front face of the calorimeter is used to take into account the extra energy clustered in jets due to neutral particles coming from pileup. Jet energy corrections are obtained from simulation and from dijet and photon+jet events in data, as discussed in ref. [50]. Additional quality criteria are applied to the jets to remove spurious jet-like features originating from isolated noise patterns in the calorimeters or the tracker. The efficiency of these requirements for signal events is above 99%. In the $\ell\nu$+jet channel, the AK8 and AK4 jets are required to be separated from any well-identified muon or electron by $\Delta R = \sqrt{(\Delta\phi)^2 + (\Delta\eta)^2} > 0.8$ and >0.3, respectively. All AK4 and AK8 jets must have $p_T > 30\,\text{GeV}$ and $>200\,\text{GeV}$, respectively, and $|\eta| < 2.4$ to be considered in the subsequent steps of the analysis.

4.3 Final reconstruction and selection of leptons and missing transverse momentum

Muons are reconstructed through a fit to hits in both the inner tracking system and the muon spectrometer [51]. Muons must satisfy identification requirements on the impact parameters of the track, the number of hits reconstructed in both the silicon tracker and the muon detectors, and the uncertainty in the p_T. These quality criteria ensure a precise measurement of the four-momentum and rejection of misreconstructed muons. An isolation requirement is applied to suppress background from multijet events where jet constituents are identified as muons. A cone of radius $\Delta R = 0.3$ is constructed around the muon direction, and the isolation parameter is defined as the scalar sum of the p_T of all the additional reconstructed tracks within the cone, divided by the muon p_T. The efficiency of this muon selection has been measured through a "tag-and-probe" method using Z bosons [43], and it has a negligible dependence on the pileup. In the high-mass $\ell\nu$+jet analysis, events must have exactly one isolated muon with $p_\mathrm{T} > 53\,\mathrm{GeV}$ and $|\eta| < 2.1$. A looser p_T requirement of 40 GeV is used for the low resonance mass range.

Electron candidates are required to have a match between energy deposited in the ECAL and momentum determined from the reconstructed track [52]. To suppress multijet background, electron candidates must pass stringent identification and isolation criteria [53]. Those criteria include requirements on the geometrical matching between ECAL depositions and position of reconstructed tracks, the ratio of the energies deposited in the HCAL and ECAL, the distribution of the ECAL depositions, the impact parameters of the track, and the number of reconstructed hits in the silicon tracker. In the high-mass $\ell\nu$+jet analysis, we require exactly one electron with $p_\mathrm{T} > 120\,\mathrm{GeV}$ and $|\eta| < 2.5$. A looser p_T requirement of 45 GeV is used for the low resonance mass range. Reconstructed electrons must also be located outside of the transition region between the ECAL barrel and endcaps ($1.44 < |\eta| < 1.57$), because the reconstruction of an electron object in this region is not optimal.

The missing transverse momentum $p_\mathrm{T}^\mathrm{miss}$ is defined as the magnitude of the vector sum of the transverse momenta of the reconstructed PF objects. The value of $p_\mathrm{T}^\mathrm{miss}$ is modified to account for corrections to the energy scale of all the reconstructed AK4 jets in the event. More details on the $p_\mathrm{T}^\mathrm{miss}$ performance in CMS can be found in refs. [54, 55]. Requirements of $p_\mathrm{T}^\mathrm{miss} > 40$ and $> 80\,\mathrm{GeV}$ are applied, respectively, in the muon and electron channels in the $\ell\nu$+jet analysis. The threshold is higher in the electron channel to further suppress the larger background from multijet processes. Since the $p_\mathrm{T}^\mathrm{miss}$ calculation requires the detector to provide complete geometric coverage, events in data without fully operational HF calorimeter are not considered for the $\ell\nu$+jet channel.

4.4 The identification of $\mathrm{W/Z} \to \mathrm{q\bar{q}}$ using jet substructure

The AK8 jets are used to reconstruct the W jet and Z jet candidates from their decays to highly boosted quark jets. To discriminate against multijet backgrounds, we exploit both the reconstructed jet mass, which is required to be close to the W or Z boson mass, and the two-prong jet substructure produced by the particle cascades of two high-p_T quarks

that merge into one jet [21]. Jets that are identified as arising from the merged decay products of a V boson are hereafter referred to as "V jets".

As a first step in exploring potential substructure, the jet constituents are subjected to a jet grooming algorithm that improves the resolution in the jet mass and reduces the effect of pileup [56]. The goal of the algorithm is to recluster the jet constituents, while applying additional requirements that eliminate soft, large-angle QCD radiation that increases the jet mass relative to the initial V boson mass. Different jet grooming algorithms have been explored at CMS, and their performance on jets in multijet processes has been studied in detail [56]. In this analysis, we use the *jet pruning* [57, 58] algorithm for the main analysis and the *jet trimming* algorithm [59] at the trigger level as well as for cross checks. Jet pruning reclusters each AK8 jet starting from all its original constituents, through the implementation of the Cambridge-Aachen (CA) algorithm [60, 61] to discard "soft" recombinations in each step of the iterative CA procedure. The pruned jet mass, m_{jet}, is computed from the sum of the four-momenta of the constituents that are not removed by the pruning; it is then scaled by the same factor as that used to correct the original jet p_{T}. The jet is considered as a V jet candidate if m_{jet} falls in the range $65 < m_{\text{jet}} < 105\,\text{GeV}$, which we define as the signal jet mass window. In the low-mass analysis, only W jet candidates are considered, thus the mass window applied is $65 < m_{\text{jet}} < 95\,\text{GeV}$.

Additional discrimination against jets from gluon and single-quark hadronization is obtained from the quantity called *N-subjettiness* [62]. The constituents of the jet before the pruning procedure are reclustered using the k_{T} algorithm [60, 63], until N joint objects (*subjets*) remain in the iterative combination procedure of the algorithm. The N-subjettiness, τ_N, is then defined as

$$\tau_N = \frac{1}{d_0} \sum_k p_{\text{T},k} \min(\Delta R_{1,k}, \Delta R_{2,k}, \ldots, \Delta R_{N,k}), \qquad (4.1)$$

where the index k runs over the PF constituents of the jet, and the distances $\Delta R_{n,k}$ are calculated relative to the axis of the n-th subjet. The normalization factor d_0 is calculated as $d_0 = \sum_k p_{\text{T},k} R_0$, setting R_0 to the distance parameter used in the clustering of the original jet. The variable τ_N quantifies the compatibility of the jet clustering with the hypothesis that exactly N subjets are present, with small values of τ_N indicating greater compatibility. The ratio between 2-subjettiness and 1-subjettiness, $\tau_{21} = \tau_2/\tau_1$, is found to be a powerful discriminant between jets originating from hadronic V decays and from gluon and single-quark hadronization. Jets from W or Z decays in signal events are characterized by lower values of τ_{21} relative to SM backgrounds. We reject V jet candidates with $\tau_{21} > 0.75$. The remaining events are further categorized according to their value of τ_{21} to enhance the sensitivity of the analysis, as summarized in table 1.

Since data/simulation discrepancies in the jet substructure variables m_{jet} and τ_{21} can bias the signal efficiency estimated from simulated samples, the modelling of signal efficiency is cross-checked in a signal-free sample with jets having characteristics that are similar to those expected for a genuine signal. A sample of high-p_{T} W bosons that decay to quarks, and are reconstructed as single AK8 jets, is studied in $t\bar{t}$ and single top quark events. Scale factors for the τ_{21} selection efficiency are extracted following ref. [21]. In this

τ_{21} selection	Efficiency scale factor
$\tau_{21} < 0.45$	0.95 ± 0.06
$0.45 < \tau_{21} < 0.75$	1.25 ± 0.32
$\tau_{21} < 0.6$	1.01 ± 0.03

Table 1. Data-to-simulation scale factors for the efficiency of the τ_{21} selection used in the analyses, as extracted from top quark enriched data and from simulation.

$\tau_{21} < 0.45$	$\langle m_{\mathrm{jet}} \rangle$ (GeV)	σ (GeV)
Data	84.6 ± 0.7	8.2 ± 0.7
Simulation	85.1 ± 0.2	7.8 ± 0.3

Table 2. The W jet mass peak position and resolution, as extracted from top quark enriched data and from simulation. These results are used to apply corrections in the V tagging procedure.

method, the pruned jet mass distributions of events that pass and fail the τ_{21} selection are fitted simultaneously to separate the W boson signal from the combinatorial components in the top quark enriched sample in both data and simulation. The scale factors are listed in table 1 and are used to correct the total signal efficiency and the VV background normalization predicted by the simulation. The uncertainties in the scale factors quoted for the τ_{21} selection include two systematic uncertainties. One comes from the modelling of the nearby jets and p_{T} spectrum in $t\bar{t}$ MC events, obtained by comparing LO and NLO $t\bar{t}$ simulation. The other is due to the choice of the models used to fit signal and background. The quadratic sum of these systematic uncertainties is found to be smaller than half of the statistical uncertainty in the scale factor. An additional uncertainty is calculated to account for the extrapolation of the scale factor from $t\bar{t}$ events with an average jet $p_{\mathrm{T}} \approx 200\,\mathrm{GeV}$ to higher momenta. This is estimated from the difference between PYTHIA and HERWIG++ [64] showering models with resulting factors of $4.5\% \ln(p_{\mathrm{T}}/200\,\mathrm{GeV})$ and $5.9\% \ln(p_{\mathrm{T}}/200\,\mathrm{GeV})$ for $\tau_{21} < 0.6$ and $\tau_{21} < 0.45$, respectively. For the $0.45 < \tau_{21} < 0.75$ selection, this uncertainty is increased by the ratio of the uncertainties in the scale factors shown in table 1 (0.32/0.06), and treated as anti-correlated with the uncertainty for $\tau_{21} < 0.45$. The mean $\langle m_{\mathrm{jet}} \rangle$ and resolution σ value of the Gaussian component of the fitted W jet mass are also extracted to obtain corrections that are applied to the simulated pruned jet mass. The values are listed in table 2, where the quoted uncertainties are statistical. The mass peak position is slightly shifted relative to the W boson mass because of the extra energy deposited in the jet cone from pileup, underlying event, and initial-state radiation not completely removed in the jet pruning procedure. For events with top quarks, additional energy contributions arise also from the possible presence of a b jet close to the W jet candidate. Because the kinematic properties of W jets and Z jets are very similar, the same corrections are also used when the V jet is assumed to arise from a Z boson.

4.5 The reconstruction and identification of W → ℓν

In the ℓν+jet channel, identified muons and electrons are associated with W → ℓν candidates. The p_T of the undetected neutrino is assumed to be equal to the p_T^{miss}. The longitudinal momentum of the neutrino (p_z) is obtained by solving a quadratic equation that sets the ℓν invariant mass to the known W boson mass [65]. In the case of two real solutions, we choose the one with smaller p_z; in the case of two complex solutions, we use their real part. The four-momentum of the neutrino is used to reconstruct the four-momentum of the W → ℓν candidate.

4.6 Final event selection and categorization

After reconstructing the two vector bosons, we apply the final criteria in the search. For all channels, any V boson candidate is required to have $p_T > 200\,\text{GeV}$. In addition, there are specific selection criteria chosen for the ℓν+jet and dijet analyses. For the ℓν+jet channel, we reject events with more than one well-identified muon or electron. We also require that the two V bosons from the decay of a massive resonance are approximately back-to-back: the ΔR between the lepton and the V jet is greater than 1.6; the $\Delta \phi$ between the vector $\vec{p}_T^{\,miss}$ and the W jet, as well as between the W → ℓν and V jet candidates, are both greater than 2 radians. To further reduce the level of the $t\bar{t}$ background in the ℓν+jet channel, events are rejected if they contain one or more b-tagged AK4 jets. This veto preserves about 90% of the signal events. For the dijet analysis, we require the two AK8 jets to have $|\Delta \eta_{jj}| < 1.3$, while the dijet system invariant mass m_{jj} must be above 1 TeV.

To enhance the analysis sensitivity, events are categorized according to the characteristics of the V jet. For the dijet and high-mass ℓν+jet channels, the V jet is deemed a W or Z boson candidate if its pruned mass falls in the range 65–85 or 85–105 GeV. This leads to three categories for the dijet channel (WW, WZ, and ZZ), and two categories for the ℓν+jet channel (WW and WZ). For the low-mass ℓν+jet channel, only W jets are considered in the signal region $65 < m_{jet} < 95\,\text{GeV}$. In addition, in the low- and high-mass ℓν+jet channels, V jets are selected to have $\tau_{21} \leq 0.45$ and ≤0.6, respectively. A tighter selection is required for the low-mass analysis as more background is expected in that mass range. In the dijet channel, we select "high-purity" (HP) and "low-purity" (LP) V jets by requiring $\tau_{21} \leq 0.45$ and $0.45 < \tau_{21} < 0.75$, respectively. Events are always required to have one HP V jet, and are divided into HP or LP events, depending on whether the other V jet is of high or low purity. Although the HP category dominates the total sensitivity of the analysis, the LP category is retained since for heavy resonances it can improve the signal efficiency with only moderate background contamination. The final categorization is therefore based on two and four classes of events for the low- and high-mass ℓν+jet channels, respectively, depending on their lepton flavor (muon or electron), and V jet mass category (W or Z). For the dijet analysis, categorization in V jet purity and mass category (WW, WZ, and ZZ) yields a total of 6 orthogonal classes of events.

The two boson candidates are combined into a diboson candidate, with presence of signal then inferred from the observation of localized excesses in the m_{VV} distribution.

Selection	Value
Lepton selections	
Electron	$p_T > 120\ (45)\,\text{GeV}$
	$\lvert\eta\rvert < 2.5\ (\text{except } 1.44 < \lvert\eta\rvert < 1.57)$
Muon	$p_T > 53\ (40)\,\text{GeV}$
	$\lvert\eta\rvert < 2.1$
Number of electrons	exactly 1
Number of muons	exactly 1
AK4 jet selections	
Jet p_T	$p_T > 30\,\text{GeV}$
Jet η	$\lvert\eta\rvert < 2.4$
Number of b-tagged AK4 jets	0
p_T^{miss} selections	
p_T^{miss} (electron channel)	$p_T^{\text{miss}} > 80\,\text{GeV}$
p_T^{miss} (muon channel)	$p_T^{\text{miss}} > 40\,\text{GeV}$
Boson selections	
$W \to \ell\nu$	$p_T > 200\,\text{GeV}$
$V \to q\bar{q}$ (AK8 jet)	$p_T > 200\,\text{GeV}$
	$\lvert\eta\rvert < 2.4$
Back-to-back topology	$\Delta R(\ell, V_{q\bar{q}}) > 1.6$
	$\Delta\phi(V_{q\bar{q}}, p_T^{\text{miss}}) > 2$
	$\Delta\phi(V_{q\bar{q}}, W_{\ell\nu}) > 2$
Pruned jet mass	$65 < m_{\text{jet}} < 105\ (95)\,\text{GeV}$
2- to 1-subjettiness ratio	$\tau_{21} < 0.60\ (0.45)$
m_{jet} categories (only for high-mass analysis)	
WW	$65 < m_{\text{jet}} < 85\,\text{GeV}$
WZ	$85 < m_{\text{jet}} < 105\,\text{GeV}$

Table 3. Summary of the final selections and categories for the $\ell\nu$+jet channel. The values indicated in parentheses correspond to the low-mass analysis.

When several diboson resonance candidates are present in the same event, only the one with the highest p_T V jet ($\ell\nu$+jet analyses) or the two highest mass V jets (dijet analysis) are retained.

A summary of the final event selections and categories is presented in table 3 for the $\ell\nu$+jet analyses and in table 4 for the dijet analysis.

Selection	Value
Boson selections	
V → qq̄ (2 AK8 jets)	$p_{\mathrm{T}} > 200\,\mathrm{GeV}$
	$|\eta| < 2.4$
Pruned jet mass	$65 < m_{\mathrm{jet}_1}, m_{\mathrm{jet}_2} < 105\,\mathrm{GeV}$
Topology	$|\Delta\eta_{\mathrm{jj}}| < 1.3$
Dijet invariant mass	$m_{\mathrm{jj}} > 1\,\mathrm{TeV}$
2- to 1-subjettiness ratio	$\tau_{21} < 0.75$
m_{jet} categories	
WW	$65 < m_{\mathrm{jet}_1} < 85\,\mathrm{GeV}$, $65 < m_{\mathrm{jet}_2} < 85\,\mathrm{GeV}$
WZ	$65 < m_{\mathrm{jet}_1} < 85\,\mathrm{GeV}$, $85 < m_{\mathrm{jet}_2} < 105\,\mathrm{GeV}$
ZZ	$85 < m_{\mathrm{jet}_1} < 105\,\mathrm{GeV}$, $85 < m_{\mathrm{jet}_2} < 105\,\mathrm{GeV}$
τ_{21} categories	
High-purity	$\tau_{21,\,\mathrm{jet}1} < 0.45$, $\tau_{21,\,\mathrm{jet}2} < 0.45$
Low-purity	$\tau_{21,\,\mathrm{jet}1} < 0.45$, $0.45 < \tau_{21,\,\mathrm{jet}2} < 0.75$

Table 4. Summary of the final selections and categories for the dijet analyses.

5 Modeling of background and signal

The m_{VV} distribution observed in data is dominated by SM background processes where single quark or gluon jets are falsely identified as V jets. Depending on the final state, the dominant processes are multijets (dijet channel) and inclusive W boson production ($\ell\nu$+jet channel). Subdominant backgrounds include $t\bar{t}$, single top quark, and nonresonant diboson SM production.

5.1 Multijet background

In the $\ell\nu$+jet channel, the multijet background is predicted to be negligible from MC simulation, whereas it represents the major contribution in the dijet analysis. For the latter, we assume that the SM background can be described by a smooth, parametrizable, monotonically decreasing distribution. The search is performed by separately fitting the background function to each search region and simultaneously adding resonant Breit-Wigner (BW) forms across all search regions to represent the signal. The background probability function is defined by empirical functional forms of 3 and 2 parameters, respectively:

$$\frac{\mathrm{d}N}{\mathrm{d}m_{\mathrm{jj}}} = \frac{P_0(1 - m_{\mathrm{jj}}/\sqrt{s})^{P_1}}{(m_{\mathrm{jj}}/\sqrt{s})^{P_2}} \qquad \text{and} \qquad \frac{\mathrm{d}N}{\mathrm{d}m_{\mathrm{jj}}} = \frac{P_0}{(m_{\mathrm{jj}}/\sqrt{s})^{P_2}}, \qquad (5.1)$$

where m_{jj} is the dijet invariant mass (equivalent to the diboson candidate mass m_{VV} for this channel), $\sqrt{s}$ is the pp collision energy in the centre of mass, P_0 is a normalization parameter, and P_1 and P_2 parametrize the shape of the m_{VV} distribution. Starting from

τ_{21} selection	Muon channel	Electron channel
$\tau_{21} < 0.6$ (high-mass)	0.87 ± 0.04	0.83 ± 0.07
$\tau_{21} < 0.45$ (low-mass)	0.85 ± 0.05	0.86 ± 0.08

Table 5. Data-to-simulation scale factors for $t\bar{t}$ and single top quark background processes, extracted from the comparison between data and simulation in the top quark enriched control sample.

the two-parameter functional form, a Fisher F-test is used to check at 10% confidence level (CL) if additional parameters are needed to model the background distribution. For the WW categories and the WZ HP category, the two-parameter form is found to describe the data spectrum sufficiently well, while for all other channels the three-parameter functional form is preferable. Alternative parametrizations and functions with up to five parameters are also studied as a cross-check.

The binning chosen for the fit reflects the detector resolution. The fit range is chosen to start where the trigger efficiency reaches its plateau, as this minimizes bias from trigger inefficiency, and to extend to the bin after the highest m_{jj} mass point. The results are shown in figure 1. The solid curve represents the maximum likelihood fit to the data, fixing the number of expected signal events to zero, while the bottom panels show the corresponding pull distributions, quantifying the agreement between the background-only fit and the data. The expected contributions from bulk graviton and W$'$ resonances with a mass of 2 TeV, scaled to their corresponding cross sections, are given by the dashed curves.

5.2 Top quark production

The backgrounds from $t\bar{t}$ and single top quark production in the $\ell\nu$+jet channel are estimated from data-based correction factors in the normalization of the simulation. A top quark enriched control sample is selected by applying all the analysis requirements in $\ell\nu$+jet events except that the b jet veto is inverted by requiring, instead, at least one b-tagged AK4 jet in the event. From the comparison between data and simulation, normalization correction factors for $t\bar{t}$ and single top quark background processes are evaluated in the pruned jet mass regions $65 < m_{jet} < 105$ GeV and $65 < m_{jet} < 95$ GeV, for the electron and muon channels, and for the low- and high-mass selections, separately. The scale factors, summarized in table 5, include both the W boson signal and the combinatorial components mainly due to events where the extra b jet from the top quark decay is in the proximity of the W, and are used to correct the normalization of the $t\bar{t}$ and single top quark simulated background predictions in the signal regions. The m_{jet} distribution in the top quark enriched sample is shown in the right plot of figure 2, while the left plot shows the τ_{21} distribution. The m_{jet} distribution shows a clear peak for events with a W boson decaying to hadrons, including the combinatorial background.

5.3 The W+jets background

The W+jets background in the $\ell\nu$+jet channel is estimated through the α *ratio method*. This method assumes that the correlation between m_{jet} and m_{VV} for the dominant W+jets
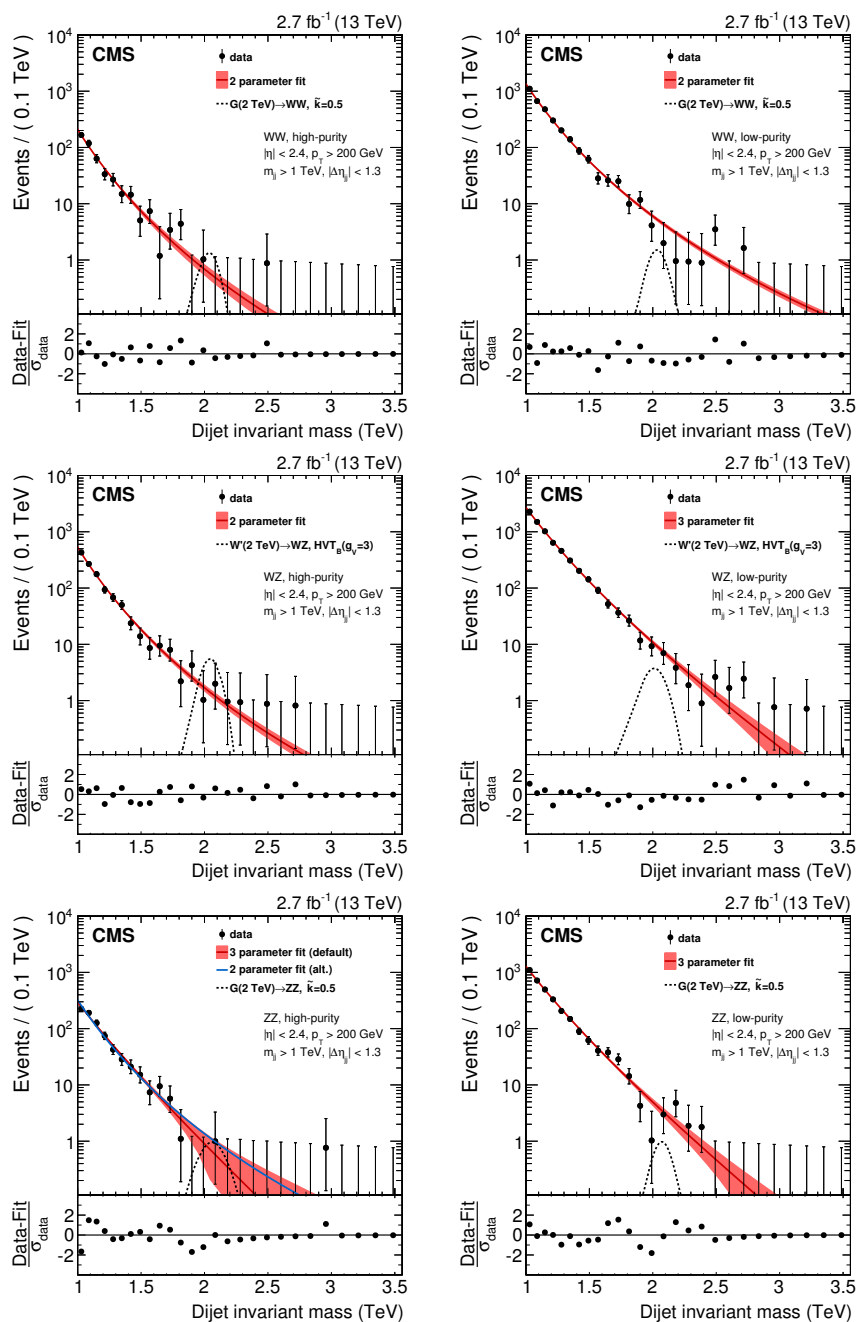
Figure 1. Final m_{jj} distributions for the dijet analysis in six signal regions. The high-purity (on the left) and the low-purity (on the right) categories are shown for the WW (top row), WZ (central row), and ZZ (bottom row) m_{jet} regions. The solid curve represents a background-only fit to the data distribution, where the filled red area corresponds to the ± 1 standard deviation statistical uncertainties of the fit. The data are represented by the black points. For the ZZ high-purity category (bottom left), we also show the background-only fit using the two-parameter functional form (blue solid line), for comparison. Signal benchmarks for a mass of 2 TeV are also shown with black dashed lines. In the lower panel of each plot, the bin-by-bin fit residuals, $(N_{\text{data}} - N_{\text{fit}})/\sigma_{\text{data}}$, are shown.
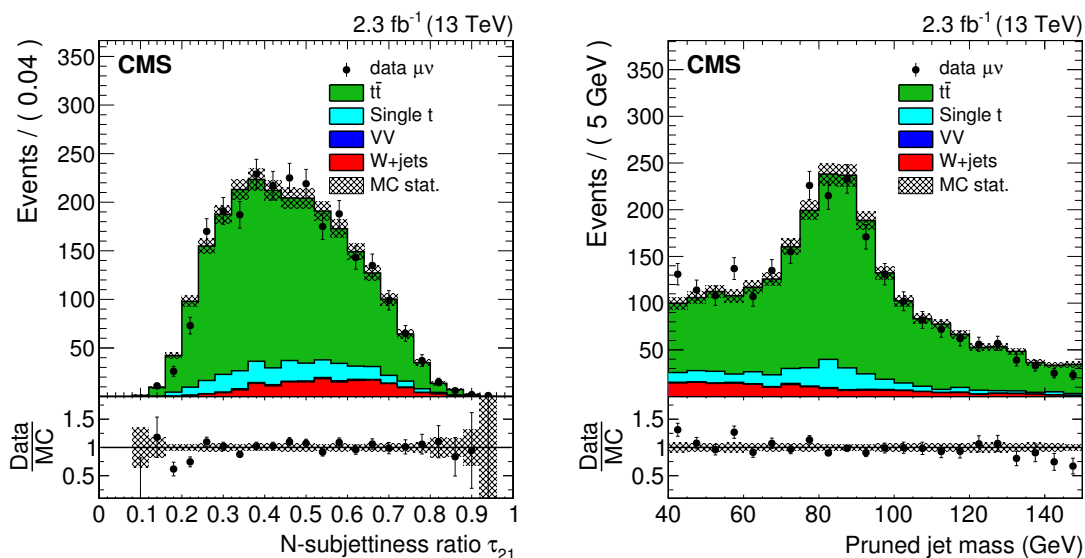
Figure 2. Distributions in N-subjettiness ratio τ_{21} (left) and pruned m_{jet} (right) from the top quark enriched control sample in the muon channel. The $t\bar{t}$ background is rescaled such that the total number of background events matches the number of events in data. In the lower panel of each plot, the ratio between data and simulation is shown together with the statistical uncertainty in the simulation normalized by its central value.

background can be adequately modelled by simulation. A signal-depleted control region (sideband) is defined by requiring the mass of the V jet to lie below or above the nominal selection; the m_{VV} distribution observed in this region is then extrapolated to the nominal region through a transfer function estimated from simulation. Other minor sources of background, such as $t\bar{t}$, single top quark, and SM diboson production, are estimated from simulation after applying correction factors based on control regions in data, as described in sections 4.4 and 5.2. The sideband region is defined around the jet mass window described in section 4. The lower and upper sidebands correspond to the m_{jet} ranges 40–65 and 135–150 GeV, respectively. The Higgs boson mass region, defined by the range 105–135 GeV, corresponds to the signal region of searches for diboson in final states with highly Lorentz-boosted Higgs bosons [66], and is therefore not used to estimate the background.

The overall normalization of the W+jets background in the signal region is determined from a fit to the m_{jet} distribution in the lower and upper sidebands of the data. The analytical form of the fitting function is chosen from simulation studies, as are the contributions from minor backgrounds. Figure 3 shows the result of this fit for the low- and high-mass $\ell\nu$+jet channels.

The form of the m_{VV} distribution for the W+jets background in the signal region (SR) is determined from the lower m_{jet} sideband (SB), through the transfer function $\alpha_{\mathrm{MC}}(m_{\mathrm{VV}})$ obtained from the W+jets simulation, and defined as:

$$\alpha_{\mathrm{MC}}(m_{\mathrm{VV}}) = \frac{F_{\mathrm{MC,SR}}^{\mathrm{W+jets}}(m_{\mathrm{VV}})}{F_{\mathrm{MC,SB}}^{\mathrm{W+jets}}(m_{\mathrm{VV}})}, \tag{5.2}$$
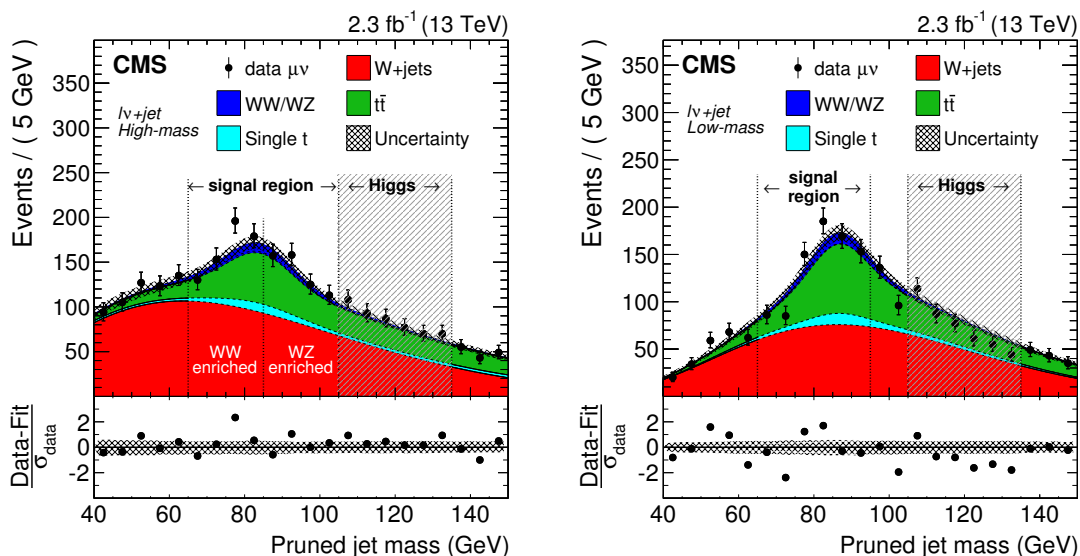
Figure 3. Distributions of the pruned jet mass m_{jet} in the $\ell\nu$+jet high-mass (left) and low-mass (right) analyses in the muon channel. All selections are applied except the requirement on m_{jet} signal window. Data are shown as black points. The signal regions and m_{jet} categories of the analyses are indicated by the vertical dotted lines. The shaded m_{jet} region 105–135 GeV is not used in these analyses. In the lower panel of each plot, the bin-by-bin fit residuals, $(N_{\mathrm{data}} - N_{\mathrm{fit}})/\sigma_{\mathrm{data}}$, are shown together with the uncertainty band of the fit normalized by the statistical uncertainty of data points, σ_{data}.

where $F(m_{\mathrm{VV}})$ is the probability density function used to describe the m_{VV} spectrum in different regions. The upper m_{jet} sideband is not considered in this fit since the expected m_{VV} distribution is different here, displaying a threshold effect not present in the lower sideband and signal regions. The adopted parameterization for the m_{VV} spectrum in both SR and SB regions is of the form $f(x) \propto \mathrm{e}^{c_0 x + c_1/x}$, which is found to adequately describe the simulation. Tests are performed with alternative functional forms, and the prediction for the backgrounds is found to agree with the one of the default function within the uncertainties.

The m_{VV} distribution observed in the lower sideband region is corrected for the presence of minor backgrounds to have an estimate of the W+jets contribution in the control region of the data, $F_{\mathrm{DATA,SB}}^{\mathrm{W+jets}}(m_{\mathrm{VV}})$. The W+jets background distribution in the signal region is then obtained by rescaling $F_{\mathrm{DATA,SB}}^{\mathrm{W+jets}}(m_{\mathrm{VV}})$ by $\alpha_{\mathrm{MC}}(m_{\mathrm{VV}})$. The minor backgrounds are then added to the W+jets background to obtain the total SM prediction in the signal region.

Figure 4 shows the final spectrum in m_{VV} for events in all categories for the low- and high-mass analyses. The observed data and the predicted background agree. The highest mass events in the $\ell\nu$+jet channel are at $m_{\mathrm{VV}} = 2.95$ and 3.15 TeV for the muon and electron categories, respectively.
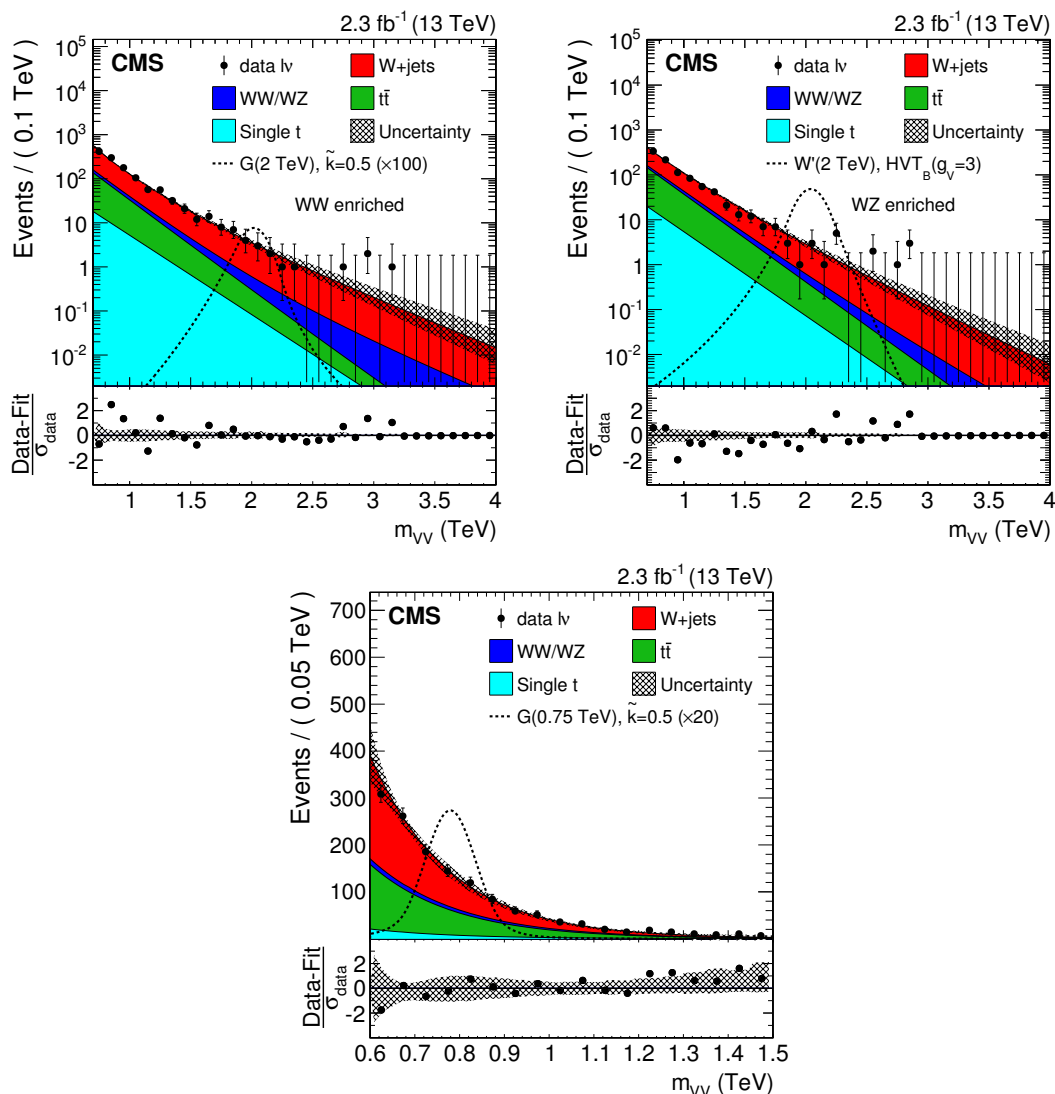
Figure 4. (Upper plots) Final m_{VV} distributions for data and expected backgrounds in the high-mass analysis obtained from the combined muon and electron channels in the WW-enriched (left) and WZ-enriched (right) signal regions. (Lower plot) Final m_{VV} distributions for data and expected backgrounds in the signal region of the low-mass analysis obtained from the combined muon and electron channels. In each plot the solid curve represents the background estimation provided by the α ratio method. The hatched band includes both statistical and systematic uncertainties. The data are shown as black points. Signal benchmarks for a mass of 2 TeV (0.75 TeV) are also shown with black dashed lines for the upper (lower) plots. In the lower panel of each plot are the bin-by-bin fit residuals, $(N_{\mathrm{data}} - N_{\mathrm{fit}})/\sigma_{\mathrm{data}}$, shown together with the uncertainty band of the fit normalized by the statistical uncertainty of data, σ_{data}.

5.4 Signal modelling

Figure 5 shows the simulated m_{jj} and $m_{\ell\nu+\mathrm{jet}}$ distributions for different resonance masses from 0.8 to 4.0 TeV. The experimental resolution for the dijet channel is around 4%, while it ranges from 6% at 1 TeV to 4% at 4 TeV in the $\ell\nu+\mathrm{jet}$ channel. We adopt an analytical
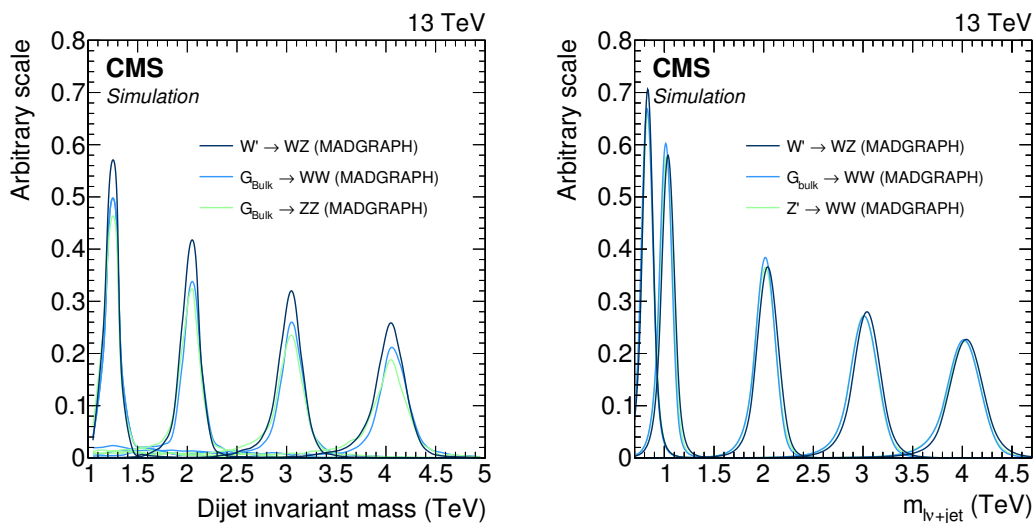
Figure 5. Dijet invariant mass (left) and $m_{\ell\nu+\text{jet}}$ (right) distributions expected for different signal mass hypotheses.

description of the signal, choosing a double-sided Crystal Ball (CB) function [67] (i.e. a Gaussian core with power law tails on both sides) to describe the simulated resonance distributions. A linear interpolation between a set of reference distributions (corresponding to masses of 0.6, 0.7, 0.8, 1.0, 1.2, 1.4, 1.6, 1.8, 2.0, 2.5, 3.0, 3.5, and 4.0 TeV) is used to estimate the expected distributions for intermediate values of resonance mass. Table 6 summarizes the overall event-selection efficiency for our chosen analysis channels and signal models. All channels are used in the statistical analysis of each signal.

6 Systematic uncertainties

6.1 Systematic uncertainties in the background estimation

For the dijet analysis, the background estimation is obtained from a fit to the data. As such, the only relevant uncertainty is the statistical one as represented by the covariance matrix of the fit to the dijet function. Different parameterizations of the fitting function have been studied, and the differences observed are well within the bounds of the aforementioned uncertainty and are assumed to pose no additional contribution.

For the $\ell\nu+$jet analyses, uncertainties in both the distribution and normalization of the background prediction can be important. The uncertainty in the distribution is dominated by the statistical uncertainties in the simultaneous fits to the data of the sideband region, and the simulation in signal and sideband regions. An effect of almost equal magnitude is due to the uncertainties in the modelling of the transfer function $\alpha(m_{\text{VV}})$ between the sideband and the signal region. The uncertainty in the normalization of the background has three sources: the W+jets component, dominated by the statistical uncertainty of the events in the pruned jet mass sideband, varying from 5 to 9%; the $t\bar{t}$/single top quark component, dominated by the scale factor obtained from the top quark enriched control

Signal	Mass (TeV)	Efficiency (%)									
		Dijet channel						$\ell\nu$+jet channel			
		WW		WZ		ZZ		WW		WZ	
		HP	LP	HP	LP	HP	LP	e	μ	e	μ
$G_{bulk} \to WW$	0.75	—	—	—	—	—	—	4.4	5.3	—	—
$G_{bulk} \to WW$	1.2	4.9	5.6	3.6	3.9	0.6	0.6	5.7	7.4	1.7	2.1
$G_{bulk} \to WW$	2.0	6.5	9.1	2.1	2.9	0.2	0.3	7.3	8.0	1.4	1.5
$G_{bulk} \to WW$	3.0	4.9	7.8	2.3	3.3	0.3	0.3	7.0	7.5	1.5	1.7
$G_{bulk} \to WW$	4.0	4.2	8.0	2.8	3.9	0.3	0.6	7.0	7.0	2.0	1.9
$G_{bulk} \to ZZ$	1.2	1.1	1.2	5.3	5.1	6.1	4.6	—	—	—	—
$G_{bulk} \to ZZ$	2.0	1.3	2.3	5.0	6.7	4.7	4.5	—	—	—	—
$G_{bulk} \to ZZ$	3.0	1.1	2.5	4.3	7.2	3.8	4.5	—	—	—	—
$G_{bulk} \to ZZ$	4.0	0.9	2.7	3.7	7.2	3.7	4.3	—	—	—	—
HVT $W' \to WZ$	0.75	—	—	—	—	—	—	1.3	1.6	—	—
HVT $W' \to WZ$	1.2	2.7	3.0	7.2	6.8	1.5	1.4	1.2	1.6	2.8	3.4
HVT $W' \to WZ$	2.0	3.0	4.7	6.0	6.7	0.8	0.8	1.8	2.0	3.0	3.3
HVT $W' \to WZ$	3.0	2.3	4.5	5.0	6.8	1.0	0.8	1.9	2.0	3.1	3.2
HVT $W' \to WZ$	4.0	1.9	4.2	4.2	6.4	1.0	1.2	1.9	2.0	3.1	3.0
HVT $Z' \to WW$	0.75	—	—	—	—	—	—	4.1	5.1	—	—
HVT $Z' \to WW$	1.2	7.2	7.6	3.3	3.6	0.4	0.4	6.0	7.7	1.6	2.0
HVT $Z' \to WW$	2.0	6.1	8.1	2.0	2.3	0.1	0.2	7.9	8.8	1.3	1.5
HVT $Z' \to WW$	3.0	4.7	8.0	2.1	2.8	0.3	0.2	7.5	8.1	1.6	1.5
HVT $Z' \to WW$	4.0	3.8	6.7	2.1	3.0	0.3	0.3	7.4	7.6	1.9	1.9

Table 6. Summary of signal efficiencies for all analysis channels and all signal models. The quoted efficiencies are in percent, and include the branching fractions of the two vector bosons to the final state of the analysis channel, effects from detector acceptance, as well as reconstruction and selection efficiencies. Values are not indicated for categories and masses where the analysis channel has no sensitivity.

region, amounting to about 5–7% and 8% in the muon and electron channels, respectively; and the diboson component, dominated by the V tagging uncertainty, which varies in the range of 3–25%.

6.2 Systematic uncertainties in the signal prediction

The dominant uncertainty in the signal selection efficiency arises from uncertainties in data-to-simulation scale factors for the V tagging efficiency derived from a top quark enriched control sample, as described in section 4.4. The normalization uncertainties are summarized in tables 7 and 8 for the dijet and $\ell\nu$+jet channels, respectively.

Uncertainties in the reconstruction of jets affect both the signal efficiency and the distribution in the reconstructed resonance mass. The four-momenta of the reconstructed jets are rescaled or smeared according to the uncertainties in the respective jet energy scale or resolution. The selection efficiencies are recalculated on these modified events,

with the resulting changes taken as systematic uncertainties that depend on the resonance mass. The induced changes on the reconstructed resonances are propagated as uncertainties in the peak position and width of the Gaussian core. In addition, the induced relative migration among V jet mass categories is evaluated, and found not to affect the overall signal efficiency. The correlations in these uncertainties between the different categories are taken into account.

The uncertainty in the lepton energy scale is correlated with the obtained signal efficiency. Changes in lepton energy are propagated to the reconstructed p_T^{miss}, and through the entire analysis. The relative change in the number of selected signal events is taken as a systematic uncertainty in the signal normalization. For both lepton flavors, the uncertainties are smaller than 1%, and are uncorrelated for different lepton flavors, but correlated for different pruned jet mass and τ_{21} categories. In addition, the induced change in peak position and its width are added as systematic uncertainties in the distribution of the signal. Again, for both lepton flavors, the uncertainties are below 1%.

The systematic uncertainties in the lepton trigger, identification, and isolation efficiencies are obtained using a tag-and-probe method in $Z \to \ell\ell$ events [43], and are used only for the $\ell\nu$+jet channel. An uncertainty of 1–3% is assigned to the trigger efficiency for both lepton flavors, depending on the lepton p_T and η. For lepton identification and isolation efficiency, the systematic uncertainty is estimated to be 1–2% for the muon and 3% for electron flavors.

The 2.7% uncertainty in the integrated luminosity [45] applies to the normalization of signal events. Uncertainties in the signal yield due to the choice of PDFs and the values chosen for the factorization (μ_f) and renormalization (μ_r) scales are also taken into account. The PDF uncertainties are evaluated using the NNPDF 3.0 [36] PDFs. The uncertainty related to the choice of μ_f and μ_r scales is evaluated following the proposal in refs. [68, 69] by varying the default choice of scales in the following 6 combinations of factors: (μ_f, μ_r) $\times$ (1/2, 1/2), (1/2, 1), (1, 1/2), (2, 2), (2, 1), and (1, 2). The uncertainty in the signal cross section from the choice of PDFs and of factorization and renormalization scales ranges from 4 to 77%, and from 1 to 22%, respectively, depending on the resonance mass, particle type and its production mechanism. These uncertainties are fully correlated among the $\ell\nu$+jet and dijet channels.

Tables 7 and 8 summarize the systematic uncertainties in the dijet and $\ell\nu$+jet channels, respectively.

7 Statistical interpretation

The m_{VV} distribution observed in data and the SM background prediction are compared to check for the presence of a new resonance decaying to vector bosons. No bins with an excess with significance larger than three standard deviations are observed. We set upper limits on the production cross section of such resonances by combining the event categories of the dijet and $\ell\nu$+jet analyses. We follow the asymptotic approximation [70] of the CL_S criterion described in refs. [71, 72]. The limits computed following this approach are found to agree with the results obtained using the modified frequentist prescription [71, 72]. For each

Source	Relevant quantity	HP uncertainty (%)	LP uncertainty (%)
Jet energy scale	Resonance shape	2	2
Jet energy resolution	Resonance shape	10	10
Jet energy and m_{jet} scale	Signal yield	0.1–4	
Jet energy and m_{jet} resolution	Signal yield	0.1–1.4	
Pileup	Signal yield	2	
Integrated luminosity	Signal yield	2	
PDFs (W$'$)	Signal yield	4–19	
PDFs (Z$'$)	Signal yield	4–13	
PDFs (G$_{\text{bulk}}$)	Signal yield	9–77	
Scales (W$'$)	Signal yield	1–14	
Scales (Z$'$)	Signal yield	1–13	
Scales (G$_{\text{bulk}}$)	Signal yield	8–22	
Jet energy and m_{jet} scale	Migration	1–50	
V tagging τ_{21}	Migration	14	21
V tagging p_{T}-dependence	Migration	7–14	5–11

Table 7. Summary of the systematic uncertainties in the contribution from signal in the dijet analysis and their impact on the event yield in the signal region and on the reconstructed distribution in m_{VV} (mean and width). The last three uncertainties result in migrations between event categories, but do not affect the overall signal efficiency.

channel and each signal hypothesis a likelihood function is built from the reconstructed m_{VV} mass distribution observed in data, the background prediction, and the signal resonance shape. A maximum-likelihood fit to the data is then performed to obtain the best estimate of the signal cross section. Systematic uncertainties are profiled [73] as log-normal nuisance parameters in the statistical interpretation, and for each possible value of the fitted signal cross section they are all refitted to maximize the likelihood.
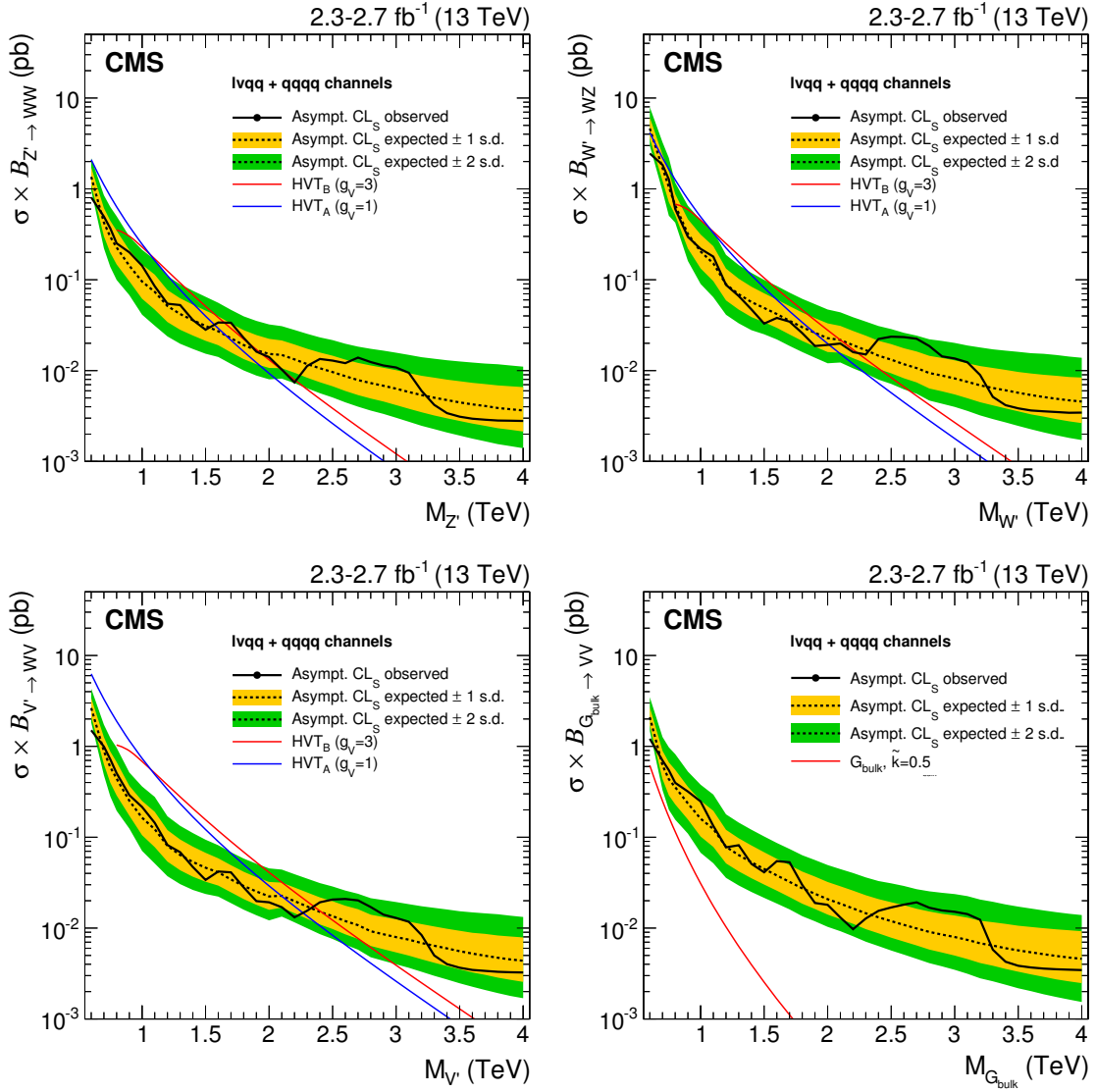
7.1 Limits on narrow-width resonance models

Exclusion limits are set in the context of the bulk graviton model and of the HVT Models A and B, under the assumption of a natural width negligible compared to the experimental resolution (narrow-width approximation). To maximize the sensitivity of the search we combine the results from all the analysis channels in each of the considered signal hypotheses. In the combination, the systematic uncertainties in jet momentum scale and resolution, V tagging efficiency scale factors, and integrated luminosity are assumed to be 100% correlated.

Figure 6 shows the resulting expected and observed exclusion limits at 95% CL on the signal cross section as a function of the resonance mass for all signal hypotheses. The limits are compared with the product of cross section and branching fraction ($\sigma \mathcal{B}$) to WW and ZZ for a bulk graviton with $k/\overline{M}_{\text{Pl}} = 0.5$, and with $\sigma \mathcal{B}$ for WZ and WW for spin-1 particles predicted by the HVT Models A and B. In this context, we consider a scenario where we expect the W$'$ and Z$'$ bosons to be degenerate in mass (triplet hypothesis). In addition, we consider also a scenario where only a charged (W$'$) or a neutral (Z$'$) resonance is expected at a given mass (singlet hypothesis). Combining the analyses leads to about 10–30%

| Source	Relevant quantity	Uncertainty (%)
Lepton trigger (μ/e)	Signal yield	1–3 / 1–3
Lepton identification (μ/e)	Signal yield	1–2 / 3
Jet energy and m_{jet} scale	Signal yield	0.2–4
Jet energy and m_{jet} resolution	Signal yield	0.1–2
Integrated luminosity	Signal yield	2.7
PDFs (W$'$)	Signal yield	4–19
PDFs (Z$'$)	Signal yield	4–13
PDFs (G$_{\mathrm{bulk}}$)	Signal yield	9–77
Scales (W$'$)	Signal yield	1–14
Scales (Z$'$)	Signal yield	1–13
Scales (G$_{\mathrm{bulk}}$)	Signal yield	8–22
Jet energy scale	Resonance shape (mean)	1.3
Jet energy scale	Resonance shape (width)	2–3
Jet energy resolution	Resonance shape (mean)	0.1
Jet energy resolution	Resonance shape (width)	4
Jet energy and m_{jet} scale	Migration	2–24
V tagging τ_{21} (0.45/0.6)	Migration	7 / 3
V tagging p_{T}-dependence (0.45/0.6)	Migration	3–6 / 6–10

Table 8. Summary of the signal systematic uncertainties for the $\ell\nu$+jet analyses and their impact on the event yield in the signal region and on the reconstructed m_{VV} shape (mean and width) for both muon and electron channels. The last three uncertainties result in migrations between event categories, but do not affect the overall signal efficiency. The correlations among different categories are taken into account.

more stringent expected upper limits on the cross section compared to the most sensitive individual channel, depending on the resonance mass and the signal hypothesis. For G$_{\mathrm{bulk}}$, Z$'$ and triplet signals (W' signal) with masses <0.8 TeV (<0.75 TeV), the limits are obtained from the low-mass $\ell\nu$+jet channel, while for the higher masses they are obtained from the high-mass $\ell\nu$+jet and dijet channels. The dijet analysis provides more stringent expected upper limits on the cross sections than the $\ell\nu$+jet analysis for resonance masses above 1.7 TeV for Z$'$ and >1.3 TeV for W$'$, because of the larger branching fractions: $\mathcal{B}(WW \to q\bar{q}q\bar{q}) = 44\%$, $\mathcal{B}(WW \to \ell\nu q\bar{q}) = 31\%$, $\mathcal{B}(WZ \to q\bar{q}q\bar{q}) = 46\%$, and $\mathcal{B}(WZ \to \ell\nu q\bar{q}) = 16\%$. In fact, the combination of high- and low-purity categories, together with the weak dependence of tagging efficiency on p_{T} [20] improves the sensitivity for most potential signal models. In the narrow-width bulk graviton model, the combined sensitivity of the searches is not large enough to set mass limits, however, cross sections are excluded in the range 3–1200 fb. For HVT Model A (B), the combined data exclude singlet W$'$ resonances with masses <2.0 (2.2) TeV and Z$'$ resonances with masses below <1.6 (1.7) TeV. Under the triplet hypothesis, spin-1 resonances with masses <2.3 and <2.4 TeV are excluded for HVT Models A and B, respectively.

Figure 6. Observed (black solid) and expected (black dashed) 95% CL upper limits on the production of a narrow-width resonance decaying to a pair of vector bosons for different signal hypotheses. In the upper plots, limits are set in the context of a spin-1 neutral Z′ (left) and charged W′ (right) resonances, and compared with the prediction of the HVT Models A and B. In the lower left plot, limits are set in the same model under the triplet hypothesis (W′ and Z′). In the lower right plot, limits are set in the context of a bulk graviton with $k/\overline{M}_{\mathrm{Pl}} = 0.5$ and compared with the prediction. For G_{bulk}, Z′ and triplet signals (W′ signal) with masses <0.8 TeV (<0.75 TeV), the limits are obtained from the low-mass $\ell\nu+$jet channel, while for the higher masses they are obtained from the high-mass $\ell\nu+$jet and dijet channels.

Figure 7 shows a scan of the coupling parameters and the corresponding observed 95% CL exclusion contours in the HVT model for the combined analyses. The parameters are defined as $g_V c_H$ and $g^2 c_F/g_V$, related to the coupling strengths of the new resonance to the Higgs boson and to fermions. The range of the scan is limited by the assumption
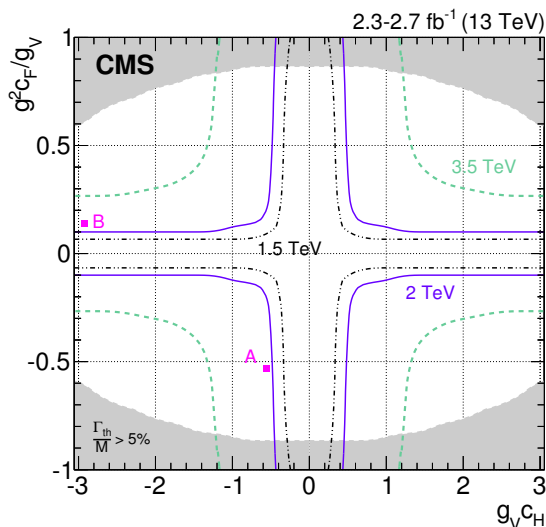
Figure 7. Exclusion regions in the plane of the HVT couplings $(g^2 c_{\mathrm{F}}/g_{\mathrm{V}}, g_{\mathrm{V}} c_{\mathrm{H}})$ for three resonance masses, 1.5, 2.0, and 3.5 TeV. Model points A and B of the benchmarks used in the analysis are also shown. The solid, dashed, and dashed-dotted lines represent the boundaries of the regions excluded by this search for different resonance masses (the region outside these lines is excluded). The areas indicated by the solid shading correspond to regions where the resonance width is predicted to be more than 5% of the resonance mass and the narrow-resonance assumption is not satisfied.

that the new resonance is narrow. A contour is overlaid, representing the region where the theoretical width is larger than the experimental resolution of the searches, and hence where the narrow-resonance assumption is not satisfied. This contour is defined by a predicted resonance width of 5%, corresponding to the narrowest resonance mass resolution of the searches.

7.2 Model-independent limits

The above analysis is specific to a narrow bulk graviton and HVT models, but these are not the only extension of the SM that predicts resonances decaying to vector bosons. It is therefore useful to reinterpret these results through a more generic model. In this section, we present the exclusion limits on the number of events that remain after modifying the analysis and greatly simplifying its structure, at a moderate cost in performance. Together with the upper limits on the number of signal events, we provide tables on reconstruction and identification efficiencies for vector bosons emitted in the kinematic acceptance of the analysis. Following the instructions detailed in appendix A, it is possible to estimate the number of events expected in a generic signal that would be detected in CMS with the present data set, and to compare it with the upper limit on the number of signal events.

To avoid the dependence on assumptions in the construction of the separate categories, we perform a simplified analysis, reducing the event classification to two ($\ell\nu$+jet) and one (dijet) categories, respectively. This is done by eliminating the low-purity categories and combining the jet mass categories in the analyses. The loss in performance is very small

for a large range of masses. The effect of dropping the LP category is observed only at very high masses, where the upper limit on the cross section becomes less stringent.

A generic model cannot be restricted to narrow signals, and we therefore provide limits as a function of both mass (M_X) and natural width (Γ_X) of the new resonance. The generated line shape is parametrized with a BW function and its full width at half maximum is defined as the Γ parameter of the BW function. The BW line shape is convolved with a double sided CB function describing the detector resolution in the $\ell\nu$+jet analysis, and with a sum of a Gaussian and CB functions for the dijet analysis. As Γ_X is varied, the parameters of the double-CB function are kept fixed to the values determined under the narrow-width approximation. It has been checked that the parametrization of detector effects factorizes from the natural width of the resonance and is stable as Γ_X increases. The width is scanned at regular steps of the relative width, Γ_X/M_X, which spans from the zero-width approximation (as in the nominal analysis), up to $\Gamma_X/M_X = 0.30$, in steps of 0.05. For high masses, the resonance shape is distorted from the BW shape owing to PDF effects creating a tail towards low masses. The line shape is corrected for this by a linear function that works well for quark induced processes. However, the shape description using this approach is unsatisfactory for gluon induced processes at very high masses and widths.

We provide the efficiency as a function of the kinematic variables of the vector boson, as the efficiency can depend significantly on the production and decay kinematic quantities of the new resonance. The efficiencies are extracted from the bulk graviton samples generated for the baseline analysis. The efficiencies are calculated by first preselecting simulated signal events according to the acceptance requirements of the analysis. The tables are therefore valid only within this kinematic region, as summarized in tables 9 and 10 of appendix A for the $\ell\nu$+jet and dijet analyses, respectively. For preselected events, the reconstructed V candidates are then required to pass all the analysis selections. The efficiencies are presented as a function of the p_T and η of the V boson prior to any simulation of detector effects. All the reweighting and rescaling effects (including lepton identification and trigger efficiencies, and V tagging scale factors) are included in the efficiencies.

The efficiencies of requiring no additional well-identified leptons and b-tagged jets in the $\ell\nu$+jet analysis are found to be independent of the diboson event kinematics. We use a constant efficiency of 95% for the combined vetoes. Similarly, the $\Delta\eta$ requirement in the dijet analysis is taken into account as a global efficiency factor of 98%.

It has been checked that the dependence of the total signal efficiency and acceptance on the width of the generated sample is very weak. We include this effect in the systematic uncertainties of the procedure, as discussed below.

Special consideration is given to cases where the boson is transversely polarized, because the calculated efficiencies are based on longitudinally polarized bosons, as in the case of the reference bulk graviton model. The efficiency of the V tagging selections depend significantly on the degree of polarization of the vector boson [21]. This effect is investigated using RS1 gravitons produced with the MADGRAPH generator. The V bosons originating from the decays of RS1 gravitons are transversely polarized in about 90% of the cases. For bosons decaying leptonically, the tables are still valid because of the generator-level selection on individual leptons, which guarantees that polarization effects for the leptonic boson
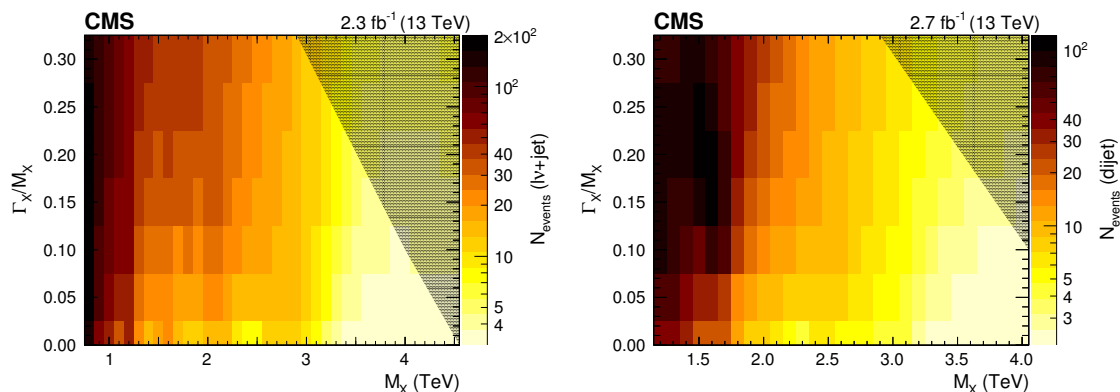
Figure 8. Observed exclusion limits at 95% CL on the number of events for a WV → ℓν + jet (left) and a VV → dijet (right) resonance, as a function of its mass and normalized width. The dark shaded area denotes the kinematic regime where the limit is valid only for the quark-antiquark annihilation processes.

are included in the acceptance. As shown in ref. [21], the efficiency of the jet substructure selection is found to be smaller for transversely polarized V bosons that tend to have more asymmetric subjet p_T, resulting in a higher probability for the subjet with lower p_T to be rejected by the pruning algorithm. Studies of simulated RS1 graviton samples show that the loss in efficiency is largely independent of the V kinematic variables, so that the effect of the transverse polarization can be adequately modelled by a constant scale factor of 0.76, independent of the p_T and η of the V → q$\overline{\text{q}}$ decays.

To validate the above procedure, the resulting parametrized efficiencies (including the event veto efficiencies) are used to predict the total efficiency for reconstructing resonances of different spin and width. The estimation is compared to the exact number obtained from performing the baseline analysis directly on the simulated events. In all cases, the agreement between the nominal and parametrized efficiencies are of the order of 10–20% for the majority of the parameter space, but grow up to 40% for very low resonance masses, were migration effects over selection boundaries cannot be treated in our parametrization approach. Various approximations and uncertainties contribute to the final additional systematic uncertainty in the efficiency; the main ones are unaccounted correlations between the physical objects, statistical uncertainties due to limited numbers of simulated events, and residual dependence on natural width. We assign an additional systematic uncertainty which ranges from 20% at high masses to 40% at low masses in the total signal efficiency for calculating the model-independent limits. This additional systematic uncertainty addresses the remaining imperfections in the parametrization of efficiencies.

Figure 8 shows the observed limits on the number of events extracted from the simplified analysis, independently for the ℓν+jet and dijet analyses, which are not combined in order to avoid assumptions on branching fractions of a resonance decaying to both WW and ZZ channels. The limits are calculated using an asymptotic approximation of the CL_S method. All systematic uncertainties considered in the baseline analysis are included in the calculation of these limits, together with the additional uncertainty related to the

approximations for parametrizing efficiencies. The main features of the observed limits presented above are still visible. With increasing width, the overall sensitivity degrades. The shaded area denotes where the limit is valid only for quark-antiquark annihilation processes, because in this region the mass distribution resulting from gluon-fusion processes can no longer be approximated by a peaking resonance.

8 Summary

A search has been presented for new resonances decaying to WW, ZZ, or WZ boson pairs in which at least one of the bosons decays into quarks. The final states involve dijet and $\ell\nu$+jet events with $\ell = \mu$ or e. The results include the W $\rightarrow \tau\nu$ contribution with subsequent decay $\tau \rightarrow \ell\nu\overline{\nu}$. The W and Z bosons that decay to quarks are selected by requiring a jet with mass compatible with the W or Z boson mass, respectively. Additional information from jet substructure is used to suppress background from W+jets and multijet processes. No evidence for a signal is found. In particular, the excesses at a resonance mass of 2 TeV observed in previous searches [12, 16] are not confirmed. The result is interpreted as an upper limit on the production cross section of a narrow-width resonance as a function its mass, in the context of the bulk graviton model (with decays to WW or ZZ), heavy vector-triplet Models A and B, and W$^{'}$ and Z$'$ singlet models. The upper limits are based on the statistical combination of the two channels. For the heavy vector-triplet, we exclude W$^{'}$ and Z$'$ resonances with respective masses <2.0 and <1.6 TeV for Model A, <2.2 and <1.7 TeV for Model B. Under the triplet hypothesis, spin-1 resonances with masses below 2.3 and 2.4 TeV are excluded for heavy vector-triplet Model A and B, respectively. In the narrow-width bulk graviton model, cross sections are excluded in the range of 3–1200 fb. This is the first search for a narrow-width bulk graviton with $\tilde{k} = 0.5$ at $\sqrt{s} = 13$ TeV. Tabulated efficiencies for the reconstruction of the vector bosons within the kinematic acceptance of the analysis are also provided, allowing for a reintepretation of the exclusion limits in a generic phenomenological model.

A Instructions and additional material for generic interpretation of the results

This appendix presents a technical description of the procedure for calculating the signal yield expected to be observed in the CMS detector in a scenario with a new resonance, X, decaying to two vector bosons in the $\ell\nu$+jet final state (WW, WZ), as well as the dijet final state (WW, WZ, and ZZ). The efficiencies are calculated using the reference bulk graviton samples described in section 3 and listed in tables 11–13.

These efficiencies can be applied to a generic model with the following procedure:

1. Generate a sample of events for a given mass and width of the X resonance; the simulated process must include the decay of the X resonance to leptons and quarks (including $W \to \tau\nu \to \ell\nu\nu$ decays).

2. Split the sample into $\ell\nu$+jet and dijet decays.

3. Filter the events according to the criteria listed in table 9 (for $\ell\nu$+jet WW decays) and table 10 (for dijet WW decays). If the resonance decays to WZ $\to \ell\nu q\bar{q}$, the criteria for a hadronically decaying W boson in table 9 should be applied to the generated

Objects	Requirements
Muons	$p_{\mathrm{T}} > 53\,\mathrm{GeV}$
	$|\eta| < 2.1$
Electrons	$p_{\mathrm{T}} > 120\,\mathrm{GeV}$
	$|\eta| < 2.5$
$\sum \vec{p}_{\mathrm{T},\nu}$	$p_{\mathrm{T}} > 40\,\mathrm{GeV}$ (muon channel)
	$p_{\mathrm{T}} > 80\,\mathrm{GeV}$ (electron channel)
$\mathrm{W} \to \ell\nu$ or $\mathrm{W} \to \tau\nu \to \ell\nu\nu\nu$	$p_{\mathrm{T}} > 200\,\mathrm{GeV}$
$\mathrm{V} \to \mathrm{q\bar{q}}$	$p_{\mathrm{T}} > 200\,\mathrm{GeV}$
	$|\eta| < 2.4$
WV system	$0.7 < m_{\mathrm{WV}} < 5.0\,\mathrm{TeV}$
	$\Delta\phi(\mathrm{V_{q\bar{q}}}, \mathrm{W}_{l\nu}) > 2$
	$\Delta\phi(\mathrm{V_{q\bar{q}}}, \sum \vec{p}_{\mathrm{T},\nu}) > 2$
	$\Delta R(\mathrm{V_{q\bar{q}}}, \ell) > \pi/2$

Table 9. Generator-level requirements for the $\ell\nu$+jet analysis, to be used for the computation of the efficiency parametrization. The vector sum of the transverse neutrino momenta $\sum \vec{p}_{\mathrm{T},\nu}$ is taken over all the neutrinos in the final state, coming either from $\mathrm{W} \to \ell\nu$ or $\mathrm{W} \to \tau\nu \to \ell\nu\nu\nu$ decays with $\ell = \mu$ or e.

Objects	Requirements
$\mathrm{V} \to \mathrm{q\bar{q}}$	$p_{\mathrm{T}} > 200\,\mathrm{GeV}$
	$|\eta| < 2.4$
VV system	$m_{\mathrm{VV}} > 1\,\mathrm{TeV}$
	$|\eta_{\mathrm{V_1}} - \eta_{\mathrm{V_2}}| < 1.3$

Table 10. Generator-level requirements for the dijet analysis, to be used for the computation of the efficiency parametrization.

hadronically decaying Z boson. If the resonance decays to ZW or ZZ in the dijet channel, the criteria in table 10 should be applied to the generated hadronically decaying Z bosons as well.

4. For each of the remaining events, calculate the efficiency for reconstructing the channels $\mathrm{W} \to \mu\nu$ and $\mathrm{W} \to \tau\nu \to \mu\nu\nu\nu$, and $\mathrm{W} \to \mathrm{e}\nu$ and $\mathrm{W} \to \tau\nu \to \mathrm{e}\nu\nu\nu$, using table 11. The table provides the efficiency parametrized as a function of p_{T} and η of the W.

5. In a similar way, in the $\ell\nu$+jet channel calculate the efficiency of the hadronically decaying W or Z bosons using the values in table 12. For the dijet decays, compute the efficiency for each boson from the values in table 13.

6. Weight each accepted event with the product of the two efficiencies found at steps 3 and 4. In the case of a X resonance decaying to WV ($\ell\nu$+jet channel), also multiply by the combined efficiency of the second-lepton and b jet vetoes, equal to 95%. A

p_T^W range (GeV)	W $\to \mu\nu$ and W $\to \tau\nu \to \mu\nu\nu\nu$

p_T^W range (GeV)	$	\eta_W	$ range
	0–0.2	0.2–0.4	0.4–0.6	0.6–0.8	0.8–1.0	1–1.25	1.25–1.5	1.5–2.0	2–2.5
200–250	0.82	0.79	0.79	0.80	0.85	0.82	0.81	0.82	0.78
250–300	0.89	0.90	0.88	0.86	0.90	0.86	0.91	0.86	0.91
300–400	0.90	0.89	0.90	0.90	0.89	0.90	0.89	0.90	0.87
400–500	0.88	0.89	0.91	0.90	0.88	0.89	0.90	0.89	0.89
500–600	0.90	0.90	0.92	0.90	0.88	0.89	0.91	0.87	0.88
600–700	0.91	0.90	0.92	0.91	0.88	0.90	0.92	0.88	0.87
700–800	0.91	0.89	0.92	0.91	0.89	0.89	0.91	0.90	0.82
800–1000	0.92	0.89	0.92	0.91	0.88	0.88	0.90	0.88	0.94
1000–1200	0.91	0.89	0.92	0.91	0.89	0.88	0.89	0.85	0.75
1200–1500	0.91	0.88	0.92	0.91	0.87	0.87	0.89	0.87	—
1500–2000	0.90	0.87	0.92	0.91	0.86	0.88	0.87	—	—
2000–2500	0.91	0.86	0.91	0.90	0.83	0.82	—	—	—
2500–3000	0.88	0.79	0.90	0.82	—	—	—	—	—
3000–4000	0.78	0.88	0.80	1.00	—	—	—	—	—
W $\to$ eν and W $\to \tau\nu \to$ e$\nu\nu\nu$									
200–250	0.78	0.75	0.82	0.81	0.79	0.80	0.71	0.79	0.68
250–300	0.79	0.79	0.77	0.80	0.78	0.82	0.79	0.73	0.78
300–400	0.82	0.82	0.82	0.83	0.82	0.82	0.80	0.81	0.80
400–500	0.82	0.82	0.81	0.84	0.81	0.81	0.82	0.82	0.80
500–600	0.83	0.83	0.84	0.84	0.83	0.81	0.82	0.84	0.85
600–700	0.83	0.84	0.84	0.83	0.85	0.84	0.82	0.84	0.88
700–800	0.84	0.83	0.84	0.85	0.84	0.84	0.82	0.82	0.94
800–1000	0.83	0.84	0.84	0.84	0.85	0.86	0.82	0.85	0.78
1000–1200	0.83	0.84	0.84	0.83	0.84	0.85	0.84	0.86	0.33
1200–1500	0.84	0.84	0.84	0.84	0.85	0.84	0.85	0.81	—
1500–2000	0.83	0.85	0.84	0.84	0.86	0.84	0.86	0.95	—
2000–2500	0.83	0.85	0.84	0.85	0.84	0.79	—	—	—
2500–3000	0.78	0.82	0.78	0.69	—	—	—	—	—
3000–4000	0.80	0.81	0.67	1.00	—	—	—	—	—

Table 11. Reconstruction and identification efficiency for the (upper table) W $\to \mu\nu$ and W $\to \tau\nu \to \mu\nu\nu\nu$, and (lower table) W $\to$ eν and W $\to \tau\nu \to$ e$\nu\nu\nu$ decays as function of generated p_T^W and $|\eta_W|$. Uncertainties in the efficiencies are included in the generic limit calculation as discussed in the text.

correction factor amounting to 98% should be applied to events in the dijet category to take into account the efficiency of the $\Delta\eta$ requirement.

7. The resulting sum of weighted events for the $\ell\nu$+jet and dijet subsamples, divided by the total number of events, provides an approximation to the total efficiency for the given model in each of the two channels.

The final numbers of events can be directly compared to the observed limits in figure 8 and table 14, in order to assess the exclusion power of the present data with respect to the model considered.

	$W_L \to q\bar{q}$								
p_T^W range (GeV)	$|\eta_W|$ range								
	0–0.2	0.2–0.4	0.4–0.6	0.6–0.8	0.8–1.0	1.0–1.25	1.25–1.5	1.5–2.0	2.0–2.5
200–250	0.31	0.36	0.33	0.28	0.37	0.38	0.30	0.25	0.26
250–300	0.54	0.48	0.57	0.46	0.50	0.54	0.47	0.48	0.56
300–400	0.71	0.70	0.72	0.70	0.70	0.65	0.66	0.63	0.59
400–500	0.65	0.65	0.66	0.64	0.64	0.67	0.62	0.63	0.70
500–600	0.72	0.71	0.73	0.72	0.73	0.70	0.66	0.69	0.72
600–700	0.74	0.75	0.74	0.73	0.72	0.71	0.71	0.72	0.78
700–800	0.73	0.74	0.73	0.75	0.72	0.71	0.67	0.68	0.65
800–1000	0.73	0.74	0.74	0.74	0.73	0.71	0.65	0.66	0.62
1000–1200	0.69	0.71	0.71	0.71	0.69	0.66	0.57	0.65	0.67
1200–1500	0.68	0.69	0.69	0.70	0.68	0.67	0.54	0.63	—
1500–2000	0.69	0.69	0.69	0.68	0.67	0.65	0.47	0.11	—
2000–2500	0.68	0.68	0.69	0.69	0.67	0.66	0.50	—	—
2500–3000	0.76	0.63	0.77	0.53	0.67	—	—	—	—
3000–4000	0.77	0.43	1.00	1.00	—	—	—	—	—
	$Z_L \to q\bar{q}$								
200–250	0.26	0.48	0.27	0.37	0.33	0.41	0.37	0.36	0.28
250–300	0.64	0.56	0.62	0.58	0.60	0.57	0.56	0.61	0.53
300–400	0.76	0.75	0.77	0.75	0.74	0.72	0.71	0.73	0.67
400–500	0.75	0.75	0.76	0.74	0.76	0.77	0.73	0.74	0.71
500–600	0.80	0.81	0.82	0.80	0.78	0.79	0.76	0.78	0.73
600–700	0.81	0.83	0.80	0.81	0.82	0.80	0.76	0.77	0.72
700–800	0.81	0.80	0.79	0.79	0.80	0.78	0.74	0.75	0.77
800–1000	0.81	0.81	0.81	0.81	0.79	0.77	0.72	0.74	0.72
1000–1200	0.78	0.78	0.79	0.78	0.77	0.75	0.66	0.71	0.77
1200–1500	0.77	0.77	0.76	0.77	0.75	0.73	0.60	0.65	0.66
1500–2000	0.74	0.74	0.73	0.74	0.72	0.67	0.52	0.57	—
2000–2500	0.72	0.73	0.73	0.73	0.69	0.66	0.53	—	—
2500–3000	0.80	0.85	0.69	0.76	—	—	—	—	—
3000–4000	1.0	0.50	1.0	—	—	—	—	—	—

Table 12. Reconstruction and identification efficiency for the (upper table) $W_L \to q\bar{q}$ and (lower table) $Z_L \to q\bar{q}$ decay as a function of generated p_T^V and $|\eta_V|$ applying the V tagging requirements used in the $\ell\nu$+jet analysis ($\tau_{21} < 0.6$). Uncertainties in the efficiencies are included in the generic limit calculation as discussed in the text.

The numbers provided refer to longitudinally polarized bosons. For transversely polarized bosons that decay leptonically, the same numbers are valid, as long as they are applied after the kinematic acceptance requirements. If the boson decays to quarks and has a transverse polarization, the efficiency must be scaled down by a factor of 0.76 for each hadronically decaying boson in the event.

	$W_L \to q\bar{q}$									
p_T^W range (GeV)	$|\eta_W|$ range									
	0.0–0.2	0.2–0.3	0.3–0.4	0.4–0.6	0.6–0.8	0.8–1.0	1.00–1.25	1.2–1.5	1.5–2.0	2.0–2.4
200–250	0.27	0.34	0.23	0.25	0.35	0.32	0.31	0.30	0.32	
250–300	0.55	0.50	0.55	0.51	0.54	0.58	0.52	0.56	0.54	
300–400	0.74	0.74	0.75	0.73	0.73	0.69	0.69	0.67	0.63	
400–500	0.69	0.68	0.70	0.69	0.68	0.69	0.65	0.65	0.71	
500–600	0.72	0.72	0.74	0.73	0.74	0.70	0.66	0.70	0.75	
600–700	0.74	0.75	0.75	0.74	0.73	0.72	0.71	0.73	0.78	
700–800	0.74	0.75	0.74	0.75	0.73	0.72	0.68	0.69	0.66	
800–1000	0.74	0.75	0.75	0.75	0.73	0.71	0.66	0.66	0.58	
1000–1200	0.70	0.71	0.72	0.72	0.69	0.67	0.59	0.63	0.40	
1200–1500	0.69	0.70	0.70	0.70	0.68	0.65	0.54	0.59	—	
1500–2000	0.68	0.69	0.68	0.68	0.67	0.65	0.47	—	—	
2000–2500	0.69	0.69	0.69	0.69	0.67	0.69	—	—	—	
2500–3000	0.74	0.66	0.73	0.60	—	—	—	—	—	
3000–4000	0.74	0.74	1.00	1.00	—	—	—	—	—	
	$Z_L \to q\bar{q}$									
200–250	—	—	0.25	—	—	0.50	—	0.50	—	—
250–300	0.30	—	0.33	0.25	0.18	—	0.33	0.67	—	—
300–350	0.46	0.15	0.33	0.44	0.45	0.21	0.41	0.12	0.44	—
350–400	0.38	0.40	0.47	0.47	0.43	0.41	0.26	0.35	0.36	0.50
400–500	0.50	0.46	0.51	0.47	0.45	0.51	0.41	0.38	0.45	0.59
500–600	0.59	0.60	0.61	0.60	0.58	0.55	0.52	0.44	0.51	0.67
600–700	0.63	0.61	0.62	0.59	0.59	0.56	0.50	0.45	0.48	0.53
700–800	0.60	0.62	0.61	0.60	0.60	0.58	0.50	0.40	0.41	0.75
800–1000	0.60	0.60	0.59	0.60	0.56	0.52	0.48	0.38	0.46	1.00
1000–1200	0.55	0.52	0.57	0.52	0.53	0.48	0.43	0.25	0.40	1.00
1200–1500	0.53	0.52	0.53	0.52	0.50	0.44	0.39	0.25	0.16	—
1500–2000	0.49	0.49	0.48	0.47	0.46	0.42	0.34	0.24	—	—
2000–2500	0.47	0.49	0.48	0.44	0.43	0.42	0.41	0.33	—	—
2500–3000	0.43	0.36	0.47	0.47	0.38	0.17	—	—	—	—
3000–4000	0.44	0.50	—	—	—	—	—	—	—	—

Table 13. Reconstruction and identification efficiency for the (upper table) $W_L \to q\bar{q}$ and (lower table) $Z_L \to q\bar{q}$ decays as a function of generated p_T^V and $|\eta_V|$ applying the V tagging requirements used in the dijet analysis ($\tau_{21} < 0.45$). Uncertainties in the efficiencies are included in the generic limit calculation as discussed in the text.

M_X (TeV)	$\ell\nu$+jet channel							dijet channel						
	Γ_X/M_X							Γ_X/M_X						
	0.00	0.05	0.10	0.15	0.20	0.25	0.30	0.00	0.05	0.10	0.15	0.20	0.25	0.30
0.8	139.9	173.5	189.2	192.7	185.7	173.1	157.8	—	—	—	—	—	—	—
0.9	66.9	87.8	104.4	115.5	120.4	120.6	117.1	—	—	—	—	—	—	—
1.0	46.9	61.4	72.4	81.6	87.9	91.0	91.4	—	—	—	—	—	—	—
1.1	35.2	47.1	58.2	66.7	72.2	75.3	76.3	—	—	—	—	—	—	—
1.2	50.7	56.5	59.7	62.0	63.8	65.1	65.9	38.3	61.7	88.6	84.8	84.3	82.8	78.1
1.3	22.7	29.4	34.9	40.4	45.5	49.9	53.0	39.6	54.9	68.9	77.8	82.2	83.0	79.0
1.4	15.1	20.5	26.3	32.1	37.9	43.0	46.9	29.8	41.9	57.3	66.7	82.7	86.3	85.7
1.5	18.2	22.4	27.1	32.1	37.2	41.7	45.1	19.7	31.0	45.6	89.1	127.4	116.0	93.4
1.6	20.1	24.1	28.4	33.4	38.3	42.3	44.9	22.4	34.0	65.7	114.8	100.5	90.1	77.3
1.7	14.2	19.0	24.4	30.6	36.7	41.3	44.0	22.1	29.1	57.6	70.9	70.9	64.6	57.2
1.8	11.8	17.7	24.5	31.6	37.0	40.0	40.6	13.0	15.4	24.2	34.6	40.4	41.1	39.7
1.9	11.6	16.6	23.1	29.8	35.1	38.4	39.7	7.7	11.8	17.2	23.7	27.8	29.3	29.5
2.0	14.7	20.4	26.7	32.0	35.2	36.8	37.2	7.7	10.6	14.5	18.7	21.5	23.1	23.9
2.1	15.4	20.8	26.4	30.6	32.7	33.6	33.9	6.2	9.0	12.5	15.6	17.5	18.8	19.5
2.2	13.2	18.5	23.9	27.5	29.4	30.2	30.6	5.1	7.8	10.9	13.4	15.1	15.9	16.5
2.3	9.8	15.4	20.7	24.2	26.1	27.1	27.3	4.6	7.8	10.5	12.2	13.2	13.8	14.3
2.4	7.9	13.3	18.4	21.4	23.0	24.2	25.1	5.9	8.4	10.2	11.1	11.8	12.2	12.6
2.5	8.5	13.7	17.4	19.5	20.6	21.6	22.6	6.4	8.4	9.5	10.1	10.6	11.0	11.3
2.6	11.0	14.6	16.7	18.0	18.8	19.5	20.3	5.5	7.8	8.7	9.2	9.6	9.9	10.2
2.7	11.9	14.6	16.0	16.8	17.3	17.7	18.4	4.8	7.0	7.8	8.3	8.6	8.9	9.2
2.8	12.3	14.1	15.0	15.5	16.0	16.2	16.7	4.8	6.2	6.8	7.3	7.7	8.0	8.3
2.9	11.9	13.1	13.8	14.3	14.6	14.9	15.2	4.6	5.5	6.1	6.5	6.9	7.2	7.4
3.0	9.5	11.0	11.7	12.0	12.4	12.5	12.6	4.5	5.1	5.6	5.9	6.3	6.6	6.9
3.1	7.5	9.2	10.1	10.7	11.2	11.6	11.9	4.1	4.5	4.9	5.3	5.6	5.9	6.2
3.2	5.6	7.1	8.0	8.8	9.4	9.9	10.3	2.9	3.7	4.2	4.6	5.0	5.3	5.6
3.3	4.0	5.3	6.2	7.0	7.7	8.3	8.8	2.4	3.1	3.6	4.0	4.4	4.8	5.1
3.4	3.4	4.3	5.1	5.8	6.5	7.1	7.6	2.3	2.7	3.1	3.5	4.0	4.3	4.6
3.5	3.2	3.9	4.5	5.1	5.6	6.2	6.8	2.2	2.5	2.8	3.2	3.6	3.9	4.2
3.6	3.0	3.6	4.1	4.6	5.1	5.6	6.1	2.2	2.5	2.7	3.0	3.5	3.7	4.0
3.7	3.0	3.5	3.9	4.3	4.7	5.2	5.7	2.2	2.4	2.6	2.9	3.3	3.5	3.8
4.0	3.1	3.4	3.7	4.0	4.4	4.8	5.3	2.1	2.2	2.3	2.6	3.0	3.2	3.4
4.1	3.3	3.6	3.9	4.2	4.6	5.0	5.5	—	—	—	—	—	—	—
4.5	3.4	3.7	4.0	4.3	4.8	5.3	6.1	—	—	—	—	—	—	—

Table 14. Simplified limits on the number of visible events from generic resonances decaying to pairs of V bosons in the $\ell\nu$+jet (left) and dijet (right) channels as a function of resonance mass, M_X, and normalized width, Γ_X/M_X. Shown are limits on the visible number of events at 95% CL using the asymptotic $\mathrm{CL_S}$ approach. Results with $\Gamma_X/M_X = 0$ are obtained using the resolution function only.

References

[1] K. Agashe, H. Davoudiasl, G. Perez and A. Soni, *Warped gravitons at the LHC and beyond*, *Phys. Rev.* **D 76** (2007) 036006 [`hep-ph/0701186`] [ɪɴSPIRE].

[2] A.L. Fitzpatrick, J. Kaplan, L. Randall and L.-T. Wang, *Searching for the Kaluza-Klein graviton in bulk RS models*, *JHEP* **09** (2007) 013 [`hep-ph/0701150`] [ɪɴSPIRE].

[3] O. Antipin, D. Atwood and A. Soni, *Search for RS gravitons via $W_L W_L$ decays*, *Phys. Lett.* **B 666** (2008) 155 [`arXiv:0711.3175`] [ɪɴSPIRE].

[4] L. Randall and R. Sundrum, *A Large mass hierarchy from a small extra dimension*, *Phys. Rev. Lett.* **83** (1999) 3370 [`hep-ph/9905221`] [ɪɴSPIRE].

[5] L. Randall and R. Sundrum, *An Alternative to compactification*, *Phys. Rev. Lett.* **83** (1999) 4690 [`hep-th/9906064`] [ɪɴSPIRE].

[6] D. Pappadopulo, A. Thamm, R. Torre and A. Wulzer, *Heavy vector triplets: bridging theory and data*, *JHEP* **09** (2014) 060 [`arXiv:1402.4431`] [ɪɴSPIRE].

[7] G. Altarelli, B. Mele and M. Ruiz-Altaba, *Searching for new heavy vector bosons in $p\bar{p}$ colliders*, *Z. Phys.* **C 45** (1989) 109 [*Erratum ibid.* **C 47** (1990) 676] [ɪɴSPIRE].

[8] ATLAS collaboration, *Search for new resonances decaying to a W or Z boson and a Higgs boson in the $\ell^+\ell^- b\bar{b}$, $\ell\nu b\bar{b}$ and $\nu\bar{\nu}b\bar{b}$ channels with pp collisions at $\sqrt{s} = 13\,TeV$ with the ATLAS detector*, *Phys. Lett.* **B 765** (2017) 32 [`arXiv:1607.05621`] [ɪɴSPIRE].

[9] ATLAS collaboration, *Searches for heavy diboson resonances in pp collisions at $\sqrt{s} = 13\,TeV$ with the ATLAS detector*, *JHEP* **09** (2016) 173 [`arXiv:1606.04833`] [ɪɴSPIRE].

[10] CMS collaboration, *Search for new resonances decaying via WZ to leptons in proton-proton collisions at $\sqrt{s} = 8\,TeV$*, *Phys. Lett.* **B 740** (2015) 83 [`arXiv:1407.3476`] [ɪɴSPIRE].

[11] CMS collaboration, *Search for massive resonances decaying into pairs of boosted bosons in semi-leptonic final states at $\sqrt{s} = 8\,TeV$*, *JHEP* **08** (2014) 174 [`arXiv:1405.3447`] [ɪɴSPIRE].

[12] CMS collaboration, *Search for massive resonances in dijet systems containing jets tagged as W or Z boson decays in pp collisions at $\sqrt{s} = 8\,TeV$*, *JHEP* **08** (2014) 173 [`arXiv:1405.1994`] [ɪɴSPIRE].

[13] CMS collaboration, *Search for massive WH resonances decaying into the $\ell\nu b\bar{b}$ final state at $\sqrt{s} = 8\,TeV$*, *Eur. Phys. J.* **C 76** (2016) 237 [`arXiv:1601.06431`] [ɪɴSPIRE].

[14] CMS collaboration, *Search for a massive resonance decaying into a Higgs boson and a W or Z boson in hadronic final states in proton-proton collisions at $\sqrt{s} = 8\,TeV$*, *JHEP* **02** (2016) 145 [`arXiv:1506.01443`] [ɪɴSPIRE].

[15] CMS collaboration, *Search for Narrow High-Mass Resonances in Proton-Proton Collisions at $\sqrt{s} = 8\,TeV$ Decaying to a Z and a Higgs Boson*, *Phys. Lett.* **B 748** (2015) 255 [`arXiv:1502.04994`] [ɪɴSPIRE].

[16] ATLAS collaboration, *Search for high-mass diboson resonances with boson-tagged jets in proton-proton collisions at $\sqrt{s} = 8\,TeV$ with the ATLAS detector*, *JHEP* **12** (2015) 055 [`arXiv:1506.00962`] [ɪɴSPIRE].

[17] ATLAS collaboration, *Search for production of WW/WZ resonances decaying to a lepton, neutrino and jets in pp collisions at $\sqrt{s} = 8$ TeV with the ATLAS detector*, *Eur. Phys. J.* **C 75** (2015) 209 [*Erratum ibid.* **C 75** (2015) 370] [`arXiv:1503.04677`] [ɪɴSPIRE].

[18] ATLAS collaboration, *Search for WZ resonances in the fully leptonic channel using pp collisions at $\sqrt{s} = 8$ TeV with the ATLAS detector*, *Phys. Lett.* **B 737** (2014) 223 [`arXiv:1406.4456`] [ɪɴSPIRE].

[19] ATLAS collaboration, *Search for a new resonance decaying to a W or Z boson and a Higgs boson in the $\ell\ell/\ell\nu/\nu\nu + b\bar{b}$ final states with the ATLAS detector*, *Eur. Phys. J.* **C 75** (2015) 263 [`arXiv:1503.08089`] [ɪɴSPIRE].

[20] CMS collaboration, *V Tagging Observables and Correlations*, CMS-PAS-JME-14-002 (2014).

[21] CMS collaboration, *Identification techniques for highly boosted W bosons that decay into hadrons*, *JHEP* **12** (2014) 017 [`arXiv:1410.4227`] [ɪɴSPIRE].

[22] CMS collaboration, *Particle-Flow Event Reconstruction in CMS and Performance for Jets, Taus and MET*, CMS-PAS-PFT-09-001 (2009).

[23] CMS collaboration, *Commissioning of the Particle-flow Event Reconstruction with the first LHC collisions recorded in the CMS detector*, CMS-PAS-PFT-10-001 (2010).

[24] CMS collaboration, *The CMS Experiment at the CERN LHC*, 2008 *JINST* **3** S08004 [ɪɴSPIRE].

[25] J. Alwall et al., *The automated computation of tree-level and next-to-leading order differential cross sections and their matching to parton shower simulations*, *JHEP* **07** (2014) 079 [`arXiv:1405.0301`] [ɪɴSPIRE].

[26] P. Nason, *A New method for combining NLO QCD with shower Monte Carlo algorithms*, *JHEP* **11** (2004) 040 [`hep-ph/0409146`] [ɪɴSPIRE].

[27] S. Frixione, P. Nason and C. Oleari, *Matching NLO QCD computations with Parton Shower simulations: the POWHEG method*, *JHEP* **11** (2007) 070 [`arXiv:0709.2092`] [ɪɴSPIRE].

[28] S. Alioli, P. Nason, C. Oleari and E. Re, *A general framework for implementing NLO calculations in shower Monte Carlo programs: the POWHEG BOX*, *JHEP* **06** (2010) 043 [`arXiv:1002.2581`] [ɪɴSPIRE].

[29] S. Alioli, P. Nason, C. Oleari and E. Re, *NLO single-top production matched with shower in POWHEG: s- and t-channel contributions*, *JHEP* **09** (2009) 111 [*Erratum ibid.* **1002** (2010) 011] [`arXiv:0907.4076`] [ɪɴSPIRE].

[30] E. Re, *Single-top Wt-channel production matched with parton showers using the POWHEG method*, *Eur. Phys. J.* **C 71** (2011) 1547 [`arXiv:1009.2450`] [ɪɴSPIRE].

[31] S. Alioli, S.-O. Moch and P. Uwer, *Hadronic top-quark pair-production with one jet and parton showering*, *JHEP* **01** (2012) 137 [`arXiv:1110.5251`] [ɪɴSPIRE].

[32] T. Sjöstrand, S. Mrenna and P.Z. Skands, *PYTHIA 6.4 Physics and Manual*, *JHEP* **05** (2006) 026 [`hep-ph/0603175`] [ɪɴSPIRE].

[33] T. Sjöstrand, S. Mrenna and P.Z. Skands, *A brief introduction to PYTHIA 8.1*, *Comput. Phys. Commun.* **178** (2008) 852 [`arXiv:0710.3820`] [ɪɴSPIRE].

[34] P. Skands, S. Carrazza and J. Rojo, *Tuning PYTHIA 8.1: the Monash 2013 Tune*, *Eur. Phys. J.* **C 74** (2014) 3024 [`arXiv:1404.5630`] [ɪɴSPIRE].

[35] CMS collaboration, *Event generator tunes obtained from underlying event and multiparton scattering measurements*, *Eur. Phys. J.* **C 76** (2016) 155 [`arXiv:1512.00815`] [ɪɴSPIRE].

[36] R.D. Ball et al., *Impact of Heavy Quark Masses on Parton Distributions and LHC Phenomenology*, *Nucl. Phys.* **B 849** (2011) 296 [arXiv:1101.1300] [ɪɴSPIRE].

[37] GEANT4 collaboration, S. Agostinelli et al., *GEANT4: A Simulation toolkit*, *Nucl. Instrum. Meth.* **A 506** (2003) 250 [ɪɴSPIRE].

[38] J.M. Campbell, R.K. Ellis and D.L. Rainwater, *Next-to-leading order QCD predictions for W + 2 jet and Z + 2 jet production at the CERN LHC*, *Phys. Rev.* **D 68** (2003) 094021 [hep-ph/0308195] [ɪɴSPIRE].

[39] J.M. Campbell, R.K. Ellis and C. Williams, *Vector boson pair production at the LHC*, *JHEP* **07** (2011) 018 [arXiv:1105.0020] [ɪɴSPIRE].

[40] J.M. Campbell and R.K. Ellis, *Top-quark processes at NLO in production and decay*, *J. Phys.* **G 42** (2015) 015005 [arXiv:1204.1513] [ɪɴSPIRE].

[41] J.M. Campbell, R.K. Ellis and F. Tramontano, *Single top production and decay at next-to-leading order*, *Phys. Rev.* **D 70** (2004) 094012 [hep-ph/0408158] [ɪɴSPIRE].

[42] Y. Li and F. Petriello, *Combining QCD and electroweak corrections to dilepton production in FEWZ*, *Phys. Rev.* **D 86** (2012) 094034 [arXiv:1208.5967] [ɪɴSPIRE].

[43] CMS collaboration, *Measurements of Inclusive W and Z Cross Sections in pp Collisions at $\sqrt{s} = 7\,TeV$*, *JHEP* **01** (2011) 080 [arXiv:1012.2466] [ɪɴSPIRE].

[44] CMS collaboration, *Identification of b quark jets at the CMS Experiment in the LHC Run 2*, CMS-PAS-BTV-15-001 (2016).

[45] CMS collaboration, *CMS luminosity measurement for the 2015 data-taking period*, CMS-PAS-LUM-15-001 (2015).

[46] CMS collaboration, *Description and performance of track and primary-vertex reconstruction with the CMS tracker*, 2014 *JINST* **9** P10009 [arXiv:1405.6569] [ɪɴSPIRE].

[47] M. Cacciari, G.P. Salam and G. Soyez, *FastJet User Manual*, *Eur. Phys. J.* **C 72** (2012) 1896 [arXiv:1111.6097] [ɪɴSPIRE].

[48] M. Cacciari, G.P. Salam and G. Soyez, *The Anti-k_t jet clustering algorithm*, *JHEP* **04** (2008) 063 [arXiv:0802.1189] [ɪɴSPIRE].

[49] CMS collaboration, *Identification of b-quark jets with the CMS experiment*, 2013 *JINST* **8** P04013 [arXiv:1211.4462] [ɪɴSPIRE].

[50] CMS collaboration, *Determination of Jet Energy Calibration and Transverse Momentum Resolution in CMS*, 2011 *JINST* **6** P11002 [arXiv:1107.4277] [ɪɴSPIRE].

[51] CMS collaboration, *Performance of CMS muon reconstruction in pp collision events at $\sqrt{s} = 7\,TeV$*, 2012 *JINST* **7** P10002 [arXiv:1206.4071] [ɪɴSPIRE].

[52] CMS collaboration, *Performance of Electron Reconstruction and Selection with the CMS Detector in Proton-Proton Collisions at $\sqrt{s} = 8\,TeV$*, 2015 *JINST* **10** P06005 [arXiv:1502.02701] [ɪɴSPIRE].

[53] CMS collaboration, *Search for leptonic decays of W' bosons in pp collisions at $\sqrt{s} = 7\,TeV$*, *JHEP* **08** (2012) 023 [arXiv:1204.4764] [ɪɴSPIRE].

[54] CMS collaboration, *Missing transverse energy performance of the CMS detector*, 2011 *JINST* **6** P09001 [arXiv:1106.5048] [ɪɴSPIRE].

[55] CMS collaboration, *Performance of the CMS missing transverse momentum reconstruction in pp data at $\sqrt{s} = 8\,TeV$*, 2015 *JINST* **10** P02006 [arXiv:1411.0511] [ɪɴSPIRE].

[56] CMS collaboration, *Studies of jet mass in dijet and W/Z + jet events*, *JHEP* **05** (2013) 090 [arXiv:1303.4811] [ɪɴSPIRE].

[57] S.D. Ellis, C.K. Vermilion and J.R. Walsh, *Techniques for improved heavy particle searches with jet substructure*, *Phys. Rev.* **D 80** (2009) 051501 [arXiv:0903.5081] [INSPIRE].

[58] S.D. Ellis, C.K. Vermilion and J.R. Walsh, *Recombination Algorithms and Jet Substructure: Pruning as a Tool for Heavy Particle Searches*, *Phys. Rev.* **D 81** (2010) 094023 [arXiv:0912.0033] [INSPIRE].

[59] D. Krohn, J. Thaler and L.-T. Wang, *Jet Trimming*, *JHEP* **02** (2010) 084 [arXiv:0912.1342] [INSPIRE].

[60] S. Catani, Y.L. Dokshitzer, M.H. Seymour and B.R. Webber, *Longitudinally invariant K_t clustering algorithms for hadron hadron collisions*, *Nucl. Phys.* **B 406** (1993) 187 [INSPIRE].

[61] Y.L. Dokshitzer, G.D. Leder, S. Moretti and B.R. Webber, *Better jet clustering algorithms*, *JHEP* **08** (1997) 001 [hep-ph/9707323] [INSPIRE].

[62] J. Thaler and K. Van Tilburg, *Identifying Boosted Objects with N-subjettiness*, *JHEP* **03** (2011) 015 [arXiv:1011.2268] [INSPIRE].

[63] S.D. Ellis and D.E. Soper, *Successive combination jet algorithm for hadron collisions*, *Phys. Rev.* **D 48** (1993) 3160 [hep-ph/9305266] [INSPIRE].

[64] M. Bahr et al., *HERWIG++ physics and manual*, *Eur. Phys. J.* **C 58** (2008) 639 [arXiv:0803.0883] [INSPIRE].

[65] PARTICLE DATA GROUP collaboration, K.A. Olive et al., *Review of Particle Physics*, *Chin. Phys.* **C 38** (2014) 090001 [INSPIRE].

[66] CMS collaboration, *Search for heavy resonances decaying into a vector boson and a Higgs boson in final states with charged leptons, neutrinos and b quarks*, *Phys. Lett.* **768 B** (2017) 137 [arXiv:1610.08066] [INSPIRE].

[67] M.J. Oreglia, *A study of the reactions $\psi' \to \gamma\gamma\psi$*, Ph.D. Thesis, Stanford University, Stanford U.S.A. (1980), SLAC Report SLAC-R-236.

[68] M. Cacciari, S. Frixione, M.L. Mangano, P. Nason and G. Ridolfi, *The $t\bar{t}$ cross-section at 1.8-TeV and 1.96-TeV: A Study of the systematics due to parton densities and scale dependence*, *JHEP* **04** (2004) 068 [hep-ph/0303085] [INSPIRE].

[69] S. Catani, D. de Florian, M. Grazzini and P. Nason, *Soft gluon resummation for Higgs boson production at hadron colliders*, *JHEP* **07** (2003) 028 [hep-ph/0306211] [INSPIRE].

[70] G. Cowan, K. Cranmer, E. Gross and O. Vitells, *Asymptotic formulae for likelihood-based tests of new physics*, *Eur. Phys. J.* **C 71** (2011) 1554 [*Erratum ibid.* **C 73** (2013) 2501] [arXiv:1007.1727] [INSPIRE].

[71] A.L. Read, *Presentation of search results: The CL_S technique*, *J. Phys.* **G 28** (2002) 2693 [INSPIRE].

[72] T. Junk, *Confidence level computation for combining searches with small statistics*, *Nucl. Instrum. Meth.* **A 434** (1999) 435 [hep-ex/9902006] [INSPIRE].

[73] ATLAS and CMS collaboration, *Combined Measurement of the Higgs Boson Mass in pp Collisions at $\sqrt{s} = 7$ and 8 TeV with the ATLAS and CMS Experiments*, *Phys. Rev. Lett.* **114** (2015) 191803 [arXiv:1503.07589] [INSPIRE].

The CMS collaboration

Yerevan Physics Institute, Yerevan, Armenia

A.M. Sirunyan, A. Tumasyan

Institut für Hochenergiephysik, Wien, Austria

W. Adam, E. Asilar, T. Bergauer, J. Brandstetter, E. Brondolin, M. Dragicevic, J. Erö, M. Flechl, M. Friedl, R. Frühwirth[1], V.M. Ghete, C. Hartl, N. Hörmann, J. Hrubec, M. Jeitler[1], A. König, I. Krätschmer, D. Liko, T. Matsushita, I. Mikulec, D. Rabady, N. Rad, B. Rahbaran, H. Rohringer, J. Schieck[1], J. Strauss, W. Waltenberger, C.-E. Wulz[1]

Institute for Nuclear Problems, Minsk, Belarus

V. Chekhovsky, O. Dvornikov, Y. Dydyshka, I. Emeliantchik, A. Litomin, V. Makarenko, V. Mossolov, R. Stefanovitch, J. Suarez Gonzalez, V. Zykunov

National Centre for Particle and High Energy Physics, Minsk, Belarus

N. Shumeiko

Universiteit Antwerpen, Antwerpen, Belgium

S. Alderweireldt, E.A. De Wolf, X. Janssen, J. Lauwers, M. Van De Klundert, H. Van Haevermaet, P. Van Mechelen, N. Van Remortel, A. Van Spilbeeck

Vrije Universiteit Brussel, Brussel, Belgium

S. Abu Zeid, F. Blekman, J. D'Hondt, N. Daci, I. De Bruyn, K. Deroover, S. Lowette, S. Moortgat, L. Moreels, A. Olbrechts, Q. Python, K. Skovpen, S. Tavernier, W. Van Doninck, P. Van Mulders, I. Van Parijs

Université Libre de Bruxelles, Bruxelles, Belgium

H. Brun, B. Clerbaux, G. De Lentdecker, H. Delannoy, G. Fasanella, L. Favart, R. Goldouzian, A. Grebenyuk, G. Karapostoli, T. Lenzi, A. Léonard, J. Luetic, T. Maerschalk, A. Marinov, A. Randle-conde, T. Seva, C. Vander Velde, P. Vanlaer, D. Vannerom, Q. Wang, R. Yonamine, F. Zenoni, F. Zhang[2]

Ghent University, Ghent, Belgium

A. Cimmino, T. Cornelis, D. Dobur, A. Fagot, M. Gul, I. Khvastunov, D. Poyraz, S. Salva, R. Schöfbeck, M. Tytgat, W. Van Driessche, E. Yazgan, N. Zaganidis

Université Catholique de Louvain, Louvain-la-Neuve, Belgium

H. Bakhshiansohi, C. Beluffi[3], O. Bondu, S. Brochet, G. Bruno, A. Caudron, S. De Visscher, C. Delaere, M. Delcourt, B. Francois, A. Giammanco, A. Jafari, M. Komm, G. Krintiras, V. Lemaitre, A. Magitteri, A. Mertens, M. Musich, C. Nuttens, K. Piotrzkowski, L. Quertenmont, M. Selvaggi, M. Vidal Marono, S. Wertz

Université de Mons, Mons, Belgium

N. Beliy

Centro Brasileiro de Pesquisas Fisicas, Rio de Janeiro, Brazil

W.L. Aldá Júnior, F.L. Alves, G.A. Alves, L. Brito, C. Hensel, A. Moraes, M.E. Pol, P. Rebello Teles

Universidade do Estado do Rio de Janeiro, Rio de Janeiro, Brazil

E. Belchior Batista Das Chagas, W. Carvalho, J. Chinellato[4], A. Custódio, E.M. Da Costa, G.G. Da Silveira[5], D. De Jesus Damiao, C. De Oliveira Martins, S. Fonseca De Souza, L.M. Huertas Guativa, H. Malbouisson, D. Matos Figueiredo, C. Mora Herrera, L. Mundim, H. Nogima, W.L. Prado Da Silva, A. Santoro, A. Sznajder, E.J. Tonelli Manganote[4], A. Vilela Pereira

Universidade Estadual Paulista [a], Universidade Federal do ABC [b], São Paulo, Brazil

S. Ahuja[a], C.A. Bernardes[a], S. Dogra[a], T.R. Fernandez Perez Tomei[a], E.M. Gregores[b], P.G. Mercadante[b], C.S. Moon[a], S.F. Novaes[a], Sandra S. Padula[a], D. Romero Abad[b], J.C. Ruiz Vargas[a]

Institute for Nuclear Research and Nuclear Energy, Sofia, Bulgaria

A. Aleksandrov, R. Hadjiiska, P. Iaydjiev, M. Rodozov, S. Stoykova, G. Sultanov, M. Vutova

University of Sofia, Sofia, Bulgaria

A. Dimitrov, I. Glushkov, L. Litov, B. Pavlov, P. Petkov

Beihang University, Beijing, China

W. Fang[6]

Institute of High Energy Physics, Beijing, China

M. Ahmad, J.G. Bian, G.M. Chen, H.S. Chen, M. Chen, Y. Chen[7], T. Cheng, C.H. Jiang, D. Leggat, Z. Liu, F. Romeo, M. Ruan, S.M. Shaheen, A. Spiezia, J. Tao, C. Wang, Z. Wang, H. Zhang, J. Zhao

State Key Laboratory of Nuclear Physics and Technology, Peking University, Beijing, China

Y. Ban, G. Chen, H. Huang, Q. Li, S. Liu, Y. Mao, S.J. Qian, D. Wang, Z. Xu

Universidad de Los Andes, Bogota, Colombia

C. Avila, A. Cabrera, L.F. Chaparro Sierra, C. Florez, J.P. Gomez, C.F. González Hernández, J.D. Ruiz Alvarez, J.C. Sanabria

University of Split, Faculty of Electrical Engineering, Mechanical Engineering and Naval Architecture, Split, Croatia

N. Godinovic, D. Lelas, I. Puljak, P.M. Ribeiro Cipriano, T. Sculac

University of Split, Faculty of Science, Split, Croatia

Z. Antunovic, M. Kovac

Institute Rudjer Boskovic, Zagreb, Croatia

V. Brigljevic, D. Ferencek, K. Kadija, B. Mesic, T. Susa

University of Cyprus, Nicosia, Cyprus

A. Attikis, G. Mavromanolakis, J. Mousa, C. Nicolaou, F. Ptochos, P.A. Razis, H. Rykaczewski, D. Tsiakkouri

Charles University, Prague, Czech Republic

M. Finger[8], M. Finger Jr.[8]

Universidad San Francisco de Quito, Quito, Ecuador

E. Carrera Jarrin

Academy of Scientific Research and Technology of the Arab Republic of Egypt, Egyptian Network of High Energy Physics, Cairo, Egypt

A. Ellithi Kamel[9], M.A. Mahmoud[10,11], A. Radi[11,12]

National Institute of Chemical Physics and Biophysics, Tallinn, Estonia

M. Kadastik, L. Perrini, M. Raidal, A. Tiko, C. Veelken

Department of Physics, University of Helsinki, Helsinki, Finland

P. Eerola, J. Pekkanen, M. Voutilainen

Helsinki Institute of Physics, Helsinki, Finland

J. Härkönen, T. Järvinen, V. Karimäki, R. Kinnunen, T. Lampén, K. Lassila-Perini, S. Lehti, T. Lindén, P. Luukka, J. Tuominiemi, E. Tuovinen, L. Wendland

Lappeenranta University of Technology, Lappeenranta, Finland

J. Talvitie, T. Tuuva

IRFU, CEA, Université Paris-Saclay, Gif-sur-Yvette, France

M. Besancon, F. Couderc, M. Dejardin, D. Denegri, B. Fabbro, J.L. Faure, C. Favaro, F. Ferri, S. Ganjour, S. Ghosh, A. Givernaud, P. Gras, G. Hamel de Monchenault, P. Jarry, I. Kucher, E. Locci, M. Machet, J. Malcles, J. Rander, A. Rosowsky, M. Titov, A. Zghiche

Laboratoire Leprince-Ringuet, Ecole Polytechnique, IN2P3-CNRS, Palaiseau, France

A. Abdulsalam, I. Antropov, S. Baffioni, F. Beaudette, P. Busson, L. Cadamuro, E. Chapon, C. Charlot, O. Davignon, R. Granier de Cassagnac, M. Jo, S. Lisniak, P. Miné, M. Nguyen, C. Ochando, G. Ortona, P. Paganini, P. Pigard, S. Regnard, R. Salerno, Y. Sirois, T. Strebler, Y. Yilmaz, A. Zabi

Institut Pluridisciplinaire Hubert Curien (IPHC), Université de Strasbourg, CNRS-IN2P3

J.-L. Agram[13], J. Andrea, A. Aubin, D. Bloch, J.-M. Brom, M. Buttignol, E.C. Chabert, N. Chanon, C. Collard, E. Conte[13], X. Coubez, J.-C. Fontaine[13], D. Gelé, U. Goerlach, A.-C. Le Bihan, P. Van Hove

Centre de Calcul de l'Institut National de Physique Nucleaire et de Physique des Particules, CNRS/IN2P3, Villeurbanne, France

S. Gadrat

Université de Lyon, Université Claude Bernard Lyon 1, CNRS-IN2P3, Institut de Physique Nucléaire de Lyon, Villeurbanne, France

S. Beauceron, C. Bernet, G. Boudoul, C.A. Carrillo Montoya, R. Chierici, D. Contardo, B. Courbon, P. Depasse, H. El Mamouni, J. Fan, J. Fay, S. Gascon, M. Gouzevitch,

G. Grenier, B. Ille, F. Lagarde, I.B. Laktineh, M. Lethuillier, L. Mirabito, A.L. Pequegnot, S. Perries, A. Popov[14], D. Sabes, V. Sordini, M. Vander Donckt, P. Verdier, S. Viret

Georgian Technical University, Tbilisi, Georgia

T. Toriashvili[15]

Tbilisi State University, Tbilisi, Georgia

D. Lomidze

RWTH Aachen University, I. Physikalisches Institut, Aachen, Germany

C. Autermann, S. Beranek, L. Feld, M.K. Kiesel, K. Klein, M. Lipinski, M. Preuten, C. Schomakers, J. Schulz, T. Verlage

RWTH Aachen University, III. Physikalisches Institut A, Aachen, Germany

A. Albert, M. Brodski, E. Dietz-Laursonn, D. Duchardt, M. Endres, M. Erdmann, S. Erdweg, T. Esch, R. Fischer, A. Güth, M. Hamer, T. Hebbeker, C. Heidemann, K. Hoepfner, S. Knutzen, M. Merschmeyer, A. Meyer, P. Millet, S. Mukherjee, M. Olschewski, K. Padeken, T. Pook, M. Radziej, H. Reithler, M. Rieger, F. Scheuch, L. Sonnenschein, D. Teyssier, S. Thüer

RWTH Aachen University, III. Physikalisches Institut B, Aachen, Germany

V. Cherepanov, G. Flügge, B. Kargoll, T. Kress, A. Künsken, J. Lingemann, T. Müller, A. Nehrkorn, A. Nowack, C. Pistone, O. Pooth, A. Stahl[16]

Deutsches Elektronen-Synchrotron, Hamburg, Germany

M. Aldaya Martin, T. Arndt, C. Asawatangtrakuldee, K. Beernaert, O. Behnke, U. Behrens, A.A. Bin Anuar, K. Borras[17], A. Campbell, P. Connor, C. Contreras-Campana, F. Costanza, C. Diez Pardos, G. Dolinska, G. Eckerlin, D. Eckstein, T. Eichhorn, E. Eren, E. Gallo[18], J. Garay Garcia, A. Geiser, A. Gizhko, J.M. Grados Luyando, A. Grohsjean, P. Gunnellini, A. Harb, J. Hauk, M. Hempel[19], H. Jung, A. Kalogeropoulos, O. Karacheban[19], M. Kasemann, J. Keaveney, C. Kleinwort, I. Korol, D. Krücker, W. Lange, A. Lelek, J. Leonard, K. Lipka, A. Lobanov, W. Lohmann[19], R. Mankel, I.-A. Melzer-Pellmann, A.B. Meyer, G. Mittag, J. Mnich, A. Mussgiller, E. Ntomari, D. Pitzl, R. Placakyte, A. Raspereza, B. Roland, M.Ö. Sahin, P. Saxena, T. Schoerner-Sadenius, C. Seitz, S. Spannagel, N. Stefaniuk, G.P. Van Onsem, R. Walsh, C. Wissing

University of Hamburg, Hamburg, Germany

V. Blobel, M. Centis Vignali, A.R. Draeger, T. Dreyer, E. Garutti, D. Gonzalez, J. Haller, M. Hoffmann, A. Junkes, R. Klanner, R. Kogler, N. Kovalchuk, T. Lapsien, T. Lenz, I. Marchesini, D. Marconi, M. Meyer, M. Niedziela, D. Nowatschin, F. Pantaleo[16], T. Peiffer, A. Perieanu, J. Poehlsen, C. Sander, C. Scharf, P. Schleper, A. Schmidt, S. Schumann, J. Schwandt, H. Stadie, G. Steinbrück, F.M. Stober, M. Stöver, H. Tholen, D. Troendle, E. Usai, L. Vanelderen, A. Vanhoefer, B. Vormwald

Institut für Experimentelle Kernphysik, Karlsruhe, Germany

M. Akbiyik, C. Barth, S. Baur, C. Baus, J. Berger, E. Butz, R. Caspart, T. Chwalek, F. Colombo, W. De Boer, A. Dierlamm, S. Fink, B. Freund, R. Friese, M. Giffels, A. Gilbert,

P. Goldenzweig, D. Haitz, F. Hartmann[16], S.M. Heindl, U. Husemann, I. Katkov[14], S. Kudella, H. Mildner, M.U. Mozer, Th. Müller, M. Plagge, G. Quast, K. Rabbertz, S. Röcker, F. Roscher, D. Schäfer, M. Schröder, I. Shvetsov, G. Sieber, H.J. Simonis, R. Ulrich, S. Wayand, M. Weber, T. Weiler, S. Williamson, C. Wöhrmann, R. Wolf

Institute of Nuclear and Particle Physics (INPP), NCSR Demokritos, Aghia Paraskevi, Greece

G. Anagnostou, G. Daskalakis, T. Geralis, V.A. Giakoumopoulou, A. Kyriakis, D. Loukas, I. Topsis-Giotis

National and Kapodistrian University of Athens, Athens, Greece

S. Kesisoglou, A. Panagiotou, N. Saoulidou, E. Tziaferi

University of Ioánnina, Ioánnina, Greece

I. Evangelou, G. Flouris, C. Foudas, P. Kokkas, N. Loukas, N. Manthos, I. Papadopoulos, E. Paradas

MTA-ELTE Lendület CMS Particle and Nuclear Physics Group, Eötvös Loránd University, Budapest, Hungary

N. Filipovic

Wigner Research Centre for Physics, Budapest, Hungary

G. Bencze, C. Hajdu, D. Horvath[20], F. Sikler, V. Veszpremi, G. Vesztergombi[21], A.J. Zsigmond

Institute of Nuclear Research ATOMKI, Debrecen, Hungary

N. Beni, S. Czellar, J. Karancsi[22], A. Makovec, J. Molnar, Z. Szillasi

Institute of Physics, University of Debrecen

M. Bartók[21], P. Raics, Z.L. Trocsanyi, B. Ujvari

National Institute of Science Education and Research, Bhubaneswar, India

S. Bahinipati, S. Choudhury[23], P. Mal, K. Mandal, A. Nayak[24], D.K. Sahoo, N. Sahoo, S.K. Swain

Panjab University, Chandigarh, India

S. Bansal, S.B. Beri, V. Bhatnagar, R. Chawla, U.Bhawandeep, A.K. Kalsi, A. Kaur, M. Kaur, R. Kumar, P. Kumari, A. Mehta, M. Mittal, J.B. Singh, G. Walia

University of Delhi, Delhi, India

Ashok Kumar, A. Bhardwaj, B.C. Choudhary, R.B. Garg, S. Keshri, S. Malhotra, M. Naimuddin, N. Nishu, K. Ranjan, R. Sharma, V. Sharma

Saha Institute of Nuclear Physics, Kolkata, India

R. Bhattacharya, S. Bhattacharya, K. Chatterjee, S. Dey, S. Dutt, S. Dutta, S. Ghosh, N. Majumdar, A. Modak, K. Mondal, S. Mukhopadhyay, S. Nandan, A. Purohit, A. Roy, D. Roy, S. Roy Chowdhury, S. Sarkar, M. Sharan, S. Thakur

Indian Institute of Technology Madras, Madras, India

P.K. Behera

Bhabha Atomic Research Centre, Mumbai, India

R. Chudasama, D. Dutta, V. Jha, V. Kumar, A.K. Mohanty[16], P.K. Netrakanti, L.M. Pant, P. Shukla, A. Topkar

Tata Institute of Fundamental Research-A, Mumbai, India

T. Aziz, S. Dugad, G. Kole, B. Mahakud, S. Mitra, G.B. Mohanty, B. Parida, N. Sur, B. Sutar

Tata Institute of Fundamental Research-B, Mumbai, India

S. Banerjee, S. Bhowmik[25], R.K. Dewanjee, S. Ganguly, M. Guchait, Sa. Jain, S. Kumar, M. Maity[25], G. Majumder, K. Mazumdar, T. Sarkar[25], N. Wickramage[26]

Indian Institute of Science Education and Research (IISER), Pune, India

S. Chauhan, S. Dube, V. Hegde, A. Kapoor, K. Kothekar, S. Pandey, A. Rane, S. Sharma

Institute for Research in Fundamental Sciences (IPM), Tehran, Iran

S. Chenarani[27], E. Eskandari Tadavani, S.M. Etesami[27], M. Khakzad, M. Mohammadi Najafabadi, M. Naseri, S. Paktinat Mehdiabadi[28], F. Rezaei Hosseinabadi, B. Safarzadeh[29], M. Zeinali

University College Dublin, Dublin, Ireland

M. Felcini, M. Grunewald

INFN Sezione di Bari ^{a}, Università di Bari ^{b}, Politecnico di Bari ^{c}, Bari, Italy

M. Abbrescia^{a,b}, C. Calabria^{a,b}, C. Caputo^{a,b}, A. Colaleo^a, D. Creanza^{a,c}, L. Cristella^{a,b}, N. De Filippis^{a,c}, M. De Palma^{a,b}, L. Fiore^a, G. Iaselli^{a,c}, G. Maggi^{a,c}, M. Maggi^a, G. Miniello^{a,b}, S. My^{a,b}, S. Nuzzo^{a,b}, A. Pompili^{a,b}, G. Pugliese^{a,c}, R. Radogna^{a,b}, A. Ranieri^a, G. Selvaggi^{a,b}, A. Sharma^a, L. Silvestris^{a,16}, R. Venditti^{a,b}, P. Verwilligen^a

INFN Sezione di Bologna ^{a}, Università di Bologna ^{b}, Bologna, Italy

G. Abbiendi^a, C. Battilana, D. Bonacorsi^{a,b}, S. Braibant-Giacomelli^{a,b}, L. Brigliadori^{a,b}, R. Campanini^{a,b}, P. Capiluppi^{a,b}, A. Castro^{a,b}, F.R. Cavallo^a, S.S. Chhibra^{a,b}, G. Codispoti^{a,b}, M. Cuffiani^{a,b}, G.M. Dallavalle^a, F. Fabbri^a, A. Fanfani^{a,b}, D. Fasanella^{a,b}, P. Giacomelli^a, C. Grandi^a, L. Guiducci^{a,b}, S. Marcellini^a, G. Masetti^a, A. Montanari^a, F.L. Navarria^{a,b}, A. Perrotta^a, A.M. Rossi^{a,b}, T. Rovelli^{a,b}, G.P. Siroli^{a,b}, N. Tosi^{a,b,16}

INFN Sezione di Catania ^{a}, Università di Catania ^{b}, Catania, Italy

S. Albergo^{a,b}, S. Costa^{a,b}, A. Di Mattia^a, F. Giordano^{a,b}, R. Potenza^{a,b}, A. Tricomi^{a,b}, C. Tuve^{a,b}

INFN Sezione di Firenze ^{a}, Università di Firenze ^{b}, Firenze, Italy

G. Barbagli^a, V. Ciulli^{a,b}, C. Civinini^a, R. D'Alessandro^{a,b}, E. Focardi^{a,b}, P. Lenzi^{a,b}, M. Meschini^a, S. Paoletti^a, L. Russo^{a,30}, G. Sguazzoni^a, D. Strom^a, L. Viliani^{a,b,16}

INFN Laboratori Nazionali di Frascati, Frascati, Italy

L. Benussi, S. Bianco, F. Fabbri, D. Piccolo, F. Primavera[16]

INFN Sezione di Genova ^{a}, Università di Genova ^{b}, Genova, Italy

V. Calvelli^{a,b}, F. Ferro^a, M.R. Monge^{a,b}, E. Robutti^a, S. Tosi^{a,b}

INFN Sezione di Milano-Bicocca ^{a}, Università di Milano-Bicocca ^{b}, Milano, Italy

L. Brianza^{a,b,16}, F. Brivio^{a,b}, V. Ciriolo^{a,b}, M.E. Dinardo^{a,b}, S. Fiorendi^{a,b,16}, S. Gennai^a, A. Ghezzi^{a,b}, P. Govoni^{a,b}, M. Malberti^{a,b}, S. Malvezzi^a, R.A. Manzoni^{a,b}, D. Menasce^a, L. Moroni^a, M. Paganoni^{a,b}, D. Pedrini^a, S. Pigazzini^{a,b}, S. Ragazzi^{a,b}, T. Tabarelli de Fatis^{a,b}

INFN Sezione di Napoli ^{a}, Università di Napoli 'Federico II' ^{b}, Napoli, Italy, Università della Basilicata ^{c}, Potenza, Italy, Università G. Marconi ^{d}, Roma, Italy

S. Buontempo^a, N. Cavallo^{a,c}, G. De Nardo, S. Di Guida^{a,d,16}, M. Esposito^{a,b}, F. Fabozzi^{a,c}, F. Fienga^{a,b}, A.O.M. Iorio^{a,b}, G. Lanza^a, L. Lista^a, S. Meola^{a,d,16}, P. Paolucci^{a,16}, C. Sciacca^{a,b}, F. Thyssen^a

INFN Sezione di Padova ^{a}, Università di Padova ^{b}, Padova, Italy, Università di Trento ^{c}, Trento, Italy

P. Azzi^{a,16}, N. Bacchetta^a, L. Benato^{a,b}, D. Bisello^{a,b}, A. Boletti^{a,b}, R. Carlin^{a,b}, P. Checchia^a, M. Dall'Osso^{a,b}, P. De Castro Manzano^a, T. Dorigo^a, U. Dosselli^a, F. Gasparini^{a,b}, U. Gasparini^{a,b}, A. Gozzelino^a, M. Margoni^{a,b}, A.T. Meneguzzo^{a,b}, M. Michelotto^a, J. Pazzini^{a,b}, M. Pegoraro^a, N. Pozzobon^{a,b}, P. Ronchese^{a,b}, E. Torassa^a, M. Zanetti^{a,b}, P. Zotto^{a,b}, G. Zumerle^{a,b}

INFN Sezione di Pavia ^{a}, Università di Pavia ^{b}, Pavia, Italy

A. Braghieri^a, F. Fallavollita^{a,b}, A. Magnani^{a,b}, P. Montagna^{a,b}, S.P. Ratti^{a,b}, V. Re^a, C. Riccardi^{a,b}, P. Salvini^a, I. Vai^{a,b}, P. Vitulo^{a,b}

INFN Sezione di Perugia ^{a}, Università di Perugia ^{b}, Perugia, Italy

L. Alunni Solestizi^{a,b}, G.M. Bilei^a, D. Ciangottini^{a,b}, L. Fanò^{a,b}, P. Lariccia^{a,b}, R. Leonardi^{a,b}, G. Mantovani^{a,b}, M. Menichelli^a, A. Saha^a, A. Santocchia^{a,b}

INFN Sezione di Pisa ^{a}, Università di Pisa ^{b}, Scuola Normale Superiore di Pisa ^{c}, Pisa, Italy

K. Androsov^{a,30}, P. Azzurri^{a,16}, G. Bagliesi^a, J. Bernardini^a, T. Boccali^a, R. Castaldi^a, M.A. Ciocci^{a,30}, R. Dell'Orso^a, S. Donato^{a,c}, G. Fedi, A. Giassi^a, M.T. Grippo^{a,30}, F. Ligabue^{a,c}, T. Lomtadze^a, L. Martini^{a,b}, A. Messineo^{a,b}, F. Palla^a, A. Rizzi^{a,b}, A. Savoy-Navarro^{a,31}, P. Spagnolo^a, R. Tenchini^a, G. Tonelli^{a,b}, A. Venturi^a, P.G. Verdini^a

INFN Sezione di Roma ^{a}, Università di Roma ^{b}, Roma, Italy

L. Barone^{a,b}, F. Cavallari^a, M. Cipriani^{a,b}, D. Del Re^{a,b,16}, M. Diemoz^a, S. Gelli^{a,b}, E. Longo^{a,b}, F. Margaroli^{a,b}, B. Marzocchi^{a,b}, P. Meridiani^a, G. Organtini^{a,b}, R. Paramatti^a, F. Preiato^{a,b}, S. Rahatlou^{a,b}, C. Rovelli^a, F. Santanastasio^{a,b}

INFN Sezione di Torino ^{a}, Università di Torino ^{b}, Torino, Italy, Università del Piemonte Orientale ^{c}, Novara, Italy

N. Amapane^{a,b}, R. Arcidiacono^{a,c,16}, S. Argiro^{a,b}, M. Arneodo^{a,c}, N. Bartosik^a, R. Bellan^{a,b}, C. Biino^a, N. Cartiglia^a, F. Cenna^{a,b}, M. Costa^{a,b}, R. Covarelli^{a,b}, A. Degano^{a,b}, N. Demaria^a, L. Finco^{a,b}, B. Kiani^{a,b}, C. Mariotti^a, S. Maselli^a,

E. Migliore^{a,b}, V. Monaco^{a,b}, E. Monteil^{a,b}, M. Monteno^{a}, M.M. Obertino^{a,b}, L. Pacher^{a,b}, N. Pastrone^{a}, M. Pelliccioni^{a}, G.L. Pinna Angioni^{a,b}, F. Ravera^{a,b}, A. Romero^{a,b}, M. Ruspa^{a,c}, R. Sacchi^{a,b}, K. Shchelina^{a,b}, V. Sola^{a}, A. Solano^{a,b}, A. Staiano^{a}, P. Traczyk^{a,b}

INFN Sezione di Trieste ^{a}, Università di Trieste ^{b}, Trieste, Italy

S. Belforte^{a}, M. Casarsa^{a}, F. Cossutti^{a}, G. Della Ricca^{a,b}, A. Zanetti^{a}

Kyungpook National University, Daegu, Korea

D.H. Kim, G.N. Kim, M.S. Kim, S. Lee, S.W. Lee, Y.D. Oh, S. Sekmen, D.C. Son, Y.C. Yang

Chonbuk National University, Jeonju, Korea

A. Lee

Chonnam National University, Institute for Universe and Elementary Particles, Kwangju, Korea

H. Kim

Hanyang University, Seoul, Korea

J.A. Brochero Cifuentes, T.J. Kim

Korea University, Seoul, Korea

S. Cho, S. Choi, Y. Go, D. Gyun, S. Ha, B. Hong, Y. Jo, Y. Kim, K. Lee, K.S. Lee, S. Lee, J. Lim, S.K. Park, Y. Roh

Seoul National University, Seoul, Korea

J. Almond, J. Kim, H. Lee, S.B. Oh, B.C. Radburn-Smith, S.h. Seo, U.K. Yang, H.D. Yoo, G.B. Yu

University of Seoul, Seoul, Korea

M. Choi, H. Kim, J.H. Kim, J.S.H. Lee, I.C. Park, G. Ryu, M.S. Ryu

Sungkyunkwan University, Suwon, Korea

Y. Choi, J. Goh, C. Hwang, J. Lee, I. Yu

Vilnius University, Vilnius, Lithuania

V. Dudenas, A. Juodagalvis, J. Vaitkus

National Centre for Particle Physics, Universiti Malaya, Kuala Lumpur, Malaysia

I. Ahmed, Z.A. Ibrahim, J.R. Komaragiri, M.A.B. Md Ali[32], F. Mohamad Idris[33], W.A.T. Wan Abdullah, M.N. Yusli, Z. Zolkapli

Centro de Investigacion y de Estudios Avanzados del IPN, Mexico City, Mexico

H. Castilla-Valdez, E. De La Cruz-Burelo, I. Heredia-De La Cruz[34], A. Hernandez-Almada, R. Lopez-Fernandez, R. Magaña Villalba, J. Mejia Guisao, A. Sanchez-Hernandez

Universidad Iberoamericana, Mexico City, Mexico

S. Carrillo Moreno, C. Oropeza Barrera, F. Vazquez Valencia

Benemerita Universidad Autonoma de Puebla, Puebla, Mexico

S. Carpinteyro, I. Pedraza, H.A. Salazar Ibarguen, C. Uribe Estrada

Universidad Autónoma de San Luis Potosí, San Luis Potosí, Mexico

A. Morelos Pineda

University of Auckland, Auckland, New Zealand

D. Krofcheck

University of Canterbury, Christchurch, New Zealand

P.H. Butler

National Centre for Physics, Quaid-I-Azam University, Islamabad, Pakistan

A. Ahmad, M. Ahmad, Q. Hassan, H.R. Hoorani, W.A. Khan, A. Saddique, M.A. Shah, M. Shoaib, M. Waqas

National Centre for Nuclear Research, Swierk, Poland

H. Bialkowska, M. Bluj, B. Boimska, T. Frueboes, M. Górski, M. Kazana, K. Nawrocki, K. Romanowska-Rybinska, M. Szleper, P. Zalewski

Institute of Experimental Physics, Faculty of Physics, University of Warsaw, Warsaw, Poland

K. Bunkowski, A. Byszuk[35], K. Doroba, A. Kalinowski, M. Konecki, J. Krolikowski, M. Misiura, M. Olszewski, M. Walczak

Laboratório de Instrumentação e Física Experimental de Partículas, Lisboa, Portugal

P. Bargassa, C. Beirão Da Cruz E Silva, B. Calpas, A. Di Francesco, P. Faccioli, P.G. Ferreira Parracho, M. Gallinaro, J. Hollar, N. Leonardo, L. Lloret Iglesias, M.V. Nemallapudi, J. Rodrigues Antunes, J. Seixas, O. Toldaiev, D. Vadruccio, J. Varela, P. Vischia

Joint Institute for Nuclear Research, Dubna, Russia

P. Bunin, M. Gavrilenko, I. Golutvin, I. Gorbunov, A. Kamenev, V. Karjavin, A. Lanev, A. Malakhov, V. Matveev[36,37], V. Palichik, V. Perelygin, M. Savina, S. Shmatov, S. Shulha, N. Skatchkov, V. Smirnov, N. Voytishin, A. Zarubin

Petersburg Nuclear Physics Institute, Gatchina (St. Petersburg), Russia

L. Chtchipounov, V. Golovtsov, Y. Ivanov, V. Kim[38], E. Kuznetsova[39], V. Murzin, V. Oreshkin, V. Sulimov, A. Vorobyev

Institute for Nuclear Research, Moscow, Russia

Yu. Andreev, A. Dermenev, S. Gninenko, N. Golubev, A. Karneyeu, M. Kirsanov, N. Krasnikov, A. Pashenkov, D. Tlisov, A. Toropin

Institute for Theoretical and Experimental Physics, Moscow, Russia

V. Epshteyn, V. Gavrilov, N. Lychkovskaya, V. Popov, I. Pozdnyakov, G. Safronov, A. Spiridonov, M. Toms, E. Vlasov, A. Zhokin

Moscow Institute of Physics and Technology, Moscow, Russia

A. Bylinkin[37]

National Research Nuclear University 'Moscow Engineering Physics Institute' (MEPhI), Moscow, Russia

R. Chistov[40], S. Polikarpov, E. Tarkovskii

P.N. Lebedev Physical Institute, Moscow, Russia

V. Andreev, M. Azarkin[37], I. Dremin[37], M. Kirakosyan, A. Leonidov[37], A. Terkulov

Skobeltsyn Institute of Nuclear Physics, Lomonosov Moscow State University, Moscow, Russia

A. Baskakov, A. Belyaev, E. Boos, M. Dubinin[41], L. Dudko, A. Ershov, A. Gribushin, V. Klyukhin, O. Kodolova, I. Lokhtin, I. Miagkov, S. Obraztsov, S. Petrushanko, V. Savrin, A. Snigirev

Novosibirsk State University (NSU), Novosibirsk, Russia

V. Blinov[42], Y.Skovpen[42], D. Shtol[42]

State Research Center of Russian Federation, Institute for High Energy Physics, Protvino, Russia

I. Azhgirey, I. Bayshev, S. Bitioukov, D. Elumakhov, V. Kachanov, A. Kalinin, D. Konstantinov, V. Krychkine, V. Petrov, R. Ryutin, A. Sobol, S. Troshin, N. Tyurin, A. Uzunian, A. Volkov

University of Belgrade, Faculty of Physics and Vinca Institute of Nuclear Sciences, Belgrade, Serbia

P. Adzic[43], P. Cirkovic, D. Devetak, M. Dordevic, J. Milosevic, V. Rekovic

Centro de Investigaciones Energéticas Medioambientales y Tecnológicas (CIEMAT), Madrid, Spain

J. Alcaraz Maestre, M. Barrio Luna, E. Calvo, M. Cerrada, M. Chamizo Llatas, N. Colino, B. De La Cruz, A. Delgado Peris, A. Escalante Del Valle, C. Fernandez Bedoya, J.P. Fernández Ramos, J. Flix, M.C. Fouz, P. Garcia-Abia, O. Gonzalez Lopez, S. Goy Lopez, J.M. Hernandez, M.I. Josa, E. Navarro De Martino, A. Pérez-Calero Yzquierdo, J. Puerta Pelayo, A. Quintario Olmeda, I. Redondo, L. Romero, M.S. Soares

Universidad Autónoma de Madrid, Madrid, Spain

J.F. de Trocóniz, M. Missiroli, D. Moran

Universidad de Oviedo, Oviedo, Spain

J. Cuevas, J. Fernandez Menendez, I. Gonzalez Caballero, J.R. González Fernández, E. Palencia Cortezon, S. Sanchez Cruz, I. Suárez Andrés, J.M. Vizan Garcia

Instituto de Física de Cantabria (IFCA), CSIC-Universidad de Cantabria, Santander, Spain

I.J. Cabrillo, A. Calderon, E. Curras, M. Fernandez, J. Garcia-Ferrero, G. Gomez, A. Lopez Virto, J. Marco, C. Martinez Rivero, F. Matorras, J. Piedra Gomez, T. Rodrigo, A. Ruiz-Jimeno, L. Scodellaro, N. Trevisani, I. Vila, R. Vilar Cortabitarte

CERN, European Organization for Nuclear Research, Geneva, Switzerland

D. Abbaneo, E. Auffray, G. Auzinger, M. Bachtis, P. Baillon, A.H. Ball, D. Barney, P. Bloch, A. Bocci, C. Botta, T. Camporesi, R. Castello, M. Cepeda, G. Cerminara, Y. Chen, D. d'Enterria, A. Dabrowski, V. Daponte, A. David, M. De Gruttola, A. De Roeck, E. Di Marco[44], M. Dobson, B. Dorney, T. du Pree, D. Duggan, M. Dünser, N. Dupont, A. Elliott-Peisert, P. Everaerts, S. Fartoukh, G. Franzoni, J. Fulcher, W. Funk, D. Gigi, K. Gill, M. Girone, F. Glege, D. Gulhan, S. Gundacker, M. Guthoff, P. Harris, J. Hegeman, V. Innocente, P. Janot, J. Kieseler, H. Kirschenmann, V. Knünz, A. Kornmayer[16], M.J. Kortelainen, K. Kousouris, M. Krammer[1], C. Lange, P. Lecoq, C. Lourenço, M.T. Lucchini, L. Malgeri, M. Mannelli, A. Martelli, F. Meijers, J.A. Merlin, S. Mersi, E. Meschi, P. Milenovic[45], F. Moortgat, S. Morovic, M. Mulders, H. Neugebauer, S. Orfanelli, L. Orsini, L. Pape, E. Perez, M. Peruzzi, A. Petrilli, G. Petrucciani, A. Pfeiffer, M. Pierini, A. Racz, T. Reis, G. Rolandi[46], M. Rovere, H. Sakulin, J.B. Sauvan, C. Schäfer, C. Schwick, M. Seidel, A. Sharma, P. Silva, P. Sphicas[47], J. Steggemann, M. Stoye, Y. Takahashi, M. Tosi, D. Treille, A. Triossi, A. Tsirou, V. Veckalns[48], G.I. Veres[21], M. Verweij, N. Wardle, H.K. Wöhri, A. Zagozdzinska[35], W.D. Zeuner

Paul Scherrer Institut, Villigen, Switzerland

W. Bertl, K. Deiters, W. Erdmann, R. Horisberger, Q. Ingram, H.C. Kaestli, D. Kotlinski, U. Langenegger, T. Rohe

Institute for Particle Physics, ETH Zurich, Zurich, Switzerland

F. Bachmair, L. Bäni, L. Bianchini, B. Casal, G. Dissertori, M. Dittmar, M. Donegà, C. Grab, C. Heidegger, D. Hits, J. Hoss, G. Kasieczka, W. Lustermann, B. Mangano, M. Marionneau, P. Martinez Ruiz del Arbol, M. Masciovecchio, M.T. Meinhard, D. Meister, F. Micheli, P. Musella, F. Nessi-Tedaldi, F. Pandolfi, J. Pata, F. Pauss, G. Perrin, L. Perrozzi, M. Quittnat, M. Rossini, M. Schönenberger, A. Starodumov[49], V.R. Tavolaro, K. Theofilatos, R. Wallny

Universität Zürich, Zurich, Switzerland

T.K. Aarrestad, C. Amsler[50], L. Caminada, M.F. Canelli, A. De Cosa, C. Galloni, A. Hinzmann, T. Hreus, B. Kilminster, J. Ngadiuba, D. Pinna, G. Rauco, P. Robmann, D. Salerno, Y. Yang, A. Zucchetta

National Central University, Chung-Li, Taiwan

V. Candelise, T.H. Doan, Sh. Jain, R. Khurana, M. Konyushikhin, C.M. Kuo, W. Lin, Y.J. Lu, A. Pozdnyakov, S.S. Yu

National Taiwan University (NTU), Taipei, Taiwan

Arun Kumar, P. Chang, Y.H. Chang, Y. Chao, K.F. Chen, P.H. Chen, F. Fiori, W.-S. Hou, Y. Hsiung, Y.F. Liu, R.-S. Lu, M. Miñano Moya, E. Paganis, A. Psallidas, J.f. Tsai

Chulalongkorn University, Faculty of Science, Department of Physics, Bangkok, Thailand

B. Asavapibhop, G. Singh, N. Srimanobhas, N. Suwonjandee

Cukurova University - Physics Department, Science and Art Faculty

A. Adiguzel, S. Damarseckin, Z.S. Demiroglu, C. Dozen, E. Eskut, S. Girgis, G. Gokbulut, Y. Guler, I. Hos[51], E.E. Kangal[52], O. Kara, A. Kayis Topaksu, U. Kiminsu, M. Oglakci, G. Onengut[53], K. Ozdemir[54], S. Ozturk[55], A. Polatoz, B. Tali[56], S. Turkcapar, I.S. Zorbakir, C. Zorbilmez

Middle East Technical University, Physics Department, Ankara, Turkey

B. Bilin, S. Bilmis, B. Isildak[57], G. Karapinar[58], M. Yalvac, M. Zeyrek

Bogazici University, Istanbul, Turkey

E. Gülmez, M. Kaya[59], O. Kaya[60], E.A. Yetkin[61], T. Yetkin[62]

Istanbul Technical University, Istanbul, Turkey

A. Cakir, K. Cankocak, S. Sen[63]

Institute for Scintillation Materials of National Academy of Science of Ukraine, Kharkov, Ukraine

B. Grynyov

National Scientific Center, Kharkov Institute of Physics and Technology, Kharkov, Ukraine

L. Levchuk, P. Sorokin

University of Bristol, Bristol, United Kingdom

R. Aggleton, F. Ball, L. Beck, J.J. Brooke, D. Burns, E. Clement, D. Cussans, H. Flacher, J. Goldstein, M. Grimes, G.P. Heath, H.F. Heath, J. Jacob, L. Kreczko, C. Lucas, D.M. Newbold[64], S. Paramesvaran, A. Poll, T. Sakuma, S. Seif El Nasr-storey, D. Smith, V.J. Smith

Rutherford Appleton Laboratory, Didcot, United Kingdom

K.W. Bell, A. Belyaev[65], C. Brew, R.M. Brown, L. Calligaris, D. Cieri, D.J.A. Cockerill, J.A. Coughlan, K. Harder, S. Harper, E. Olaiya, D. Petyt, C.H. Shepherd-Themistocleous, A. Thea, I.R. Tomalin, T. Williams

Imperial College, London, United Kingdom

M. Baber, R. Bainbridge, O. Buchmuller, A. Bundock, D. Burton, S. Casasso, M. Citron, D. Colling, L. Corpe, P. Dauncey, G. Davies, A. De Wit, M. Della Negra, R. Di Maria, P. Dunne, A. Elwood, D. Futyan, Y. Haddad, G. Hall, G. Iles, T. James, R. Lane, C. Laner, R. Lucas[64], L. Lyons, A.-M. Magnan, S. Malik, L. Mastrolorenzo, J. Nash, A. Nikitenko[49], J. Pela, B. Penning, M. Pesaresi, D.M. Raymond, A. Richards, A. Rose, C. Seez, S. Summers, A. Tapper, K. Uchida, M. Vazquez Acosta[66], T. Virdee[16], J. Wright, S.C. Zenz

Brunel University, Uxbridge, United Kingdom

J.E. Cole, P.R. Hobson, A. Khan, P. Kyberd, I.D. Reid, P. Symonds, L. Teodorescu, M. Turner

Baylor University, Waco, U.S.A.

A. Borzou, K. Call, J. Dittmann, K. Hatakeyama, H. Liu, N. Pastika

The University of Alabama, Tuscaloosa, U.S.A.

S.I. Cooper, C. Henderson, P. Rumerio, C. West

Boston University, Boston, U.S.A.

D. Arcaro, A. Avetisyan, T. Bose, D. Gastler, D. Rankin, C. Richardson, J. Rohlf, L. Sulak, D. Zou

Brown University, Providence, U.S.A.

G. Benelli, D. Cutts, A. Garabedian, J. Hakala, U. Heintz, J.M. Hogan, O. Jesus, K.H.M. Kwok, E. Laird, G. Landsberg, Z. Mao, M. Narain, S. Piperov, S. Sagir, E. Spencer, R. Syarif

University of California, Davis, Davis, U.S.A.

R. Breedon, D. Burns, M. Calderon De La Barca Sanchez, S. Chauhan, M. Chertok, J. Conway, R. Conway, P.T. Cox, R. Erbacher, C. Flores, G. Funk, M. Gardner, W. Ko, R. Lander, C. Mclean, M. Mulhearn, D. Pellett, J. Pilot, S. Shalhout, J. Smith, M. Squires, D. Stolp, M. Tripathi

University of California, Los Angeles, U.S.A.

C. Bravo, R. Cousins, A. Dasgupta, A. Florent, J. Hauser, M. Ignatenko, N. Mccoll, D. Saltzberg, C. Schnaible, V. Valuev, M. Weber

University of California, Riverside, Riverside, U.S.A.

E. Bouvier, K. Burt, R. Clare, J. Ellison, J.W. Gary, S.M.A. Ghiasi Shirazi, G. Hanson, J. Heilman, P. Jandir, E. Kennedy, F. Lacroix, O.R. Long, M. Olmedo Negrete, M.I. Paneva, A. Shrinivas, W. Si, H. Wei, S. Wimpenny, B. R. Yates

University of California, San Diego, La Jolla, U.S.A.

J.G. Branson, G.B. Cerati, S. Cittolin, M. Derdzinski, R. Gerosa, A. Holzner, D. Klein, V. Krutelyov, J. Letts, I. Macneill, D. Olivito, S. Padhi, M. Pieri, M. Sani, V. Sharma, S. Simon, M. Tadel, A. Vartak, S. Wasserbaech[67], C. Welke, J. Wood, F. Würthwein, A. Yagil, G. Zevi Della Porta

University of California, Santa Barbara - Department of Physics, Santa Barbara, U.S.A.

N. Amin, R. Bhandari, J. Bradmiller-Feld, C. Campagnari, A. Dishaw, V. Dutta, M. Franco Sevilla, C. George, F. Golf, L. Gouskos, J. Gran, R. Heller, J. Incandela, S.D. Mullin, A. Ovcharova, H. Qu, J. Richman, D. Stuart, I. Suarez, J. Yoo

California Institute of Technology, Pasadena, U.S.A.

D. Anderson, J. Bendavid, A. Bornheim, J. Bunn, J. Duarte, J.M. Lawhorn, A. Mott, H.B. Newman, C. Pena, M. Spiropulu, J.R. Vlimant, S. Xie, R.Y. Zhu

Carnegie Mellon University, Pittsburgh, U.S.A.

M.B. Andrews, T. Ferguson, M. Paulini, J. Russ, M. Sun, H. Vogel, I. Vorobiev, M. Weinberg

University of Colorado Boulder, Boulder, U.S.A.

J.P. Cumalat, W.T. Ford, F. Jensen, A. Johnson, M. Krohn, T. Mulholland, K. Stenson, S.R. Wagner

Cornell University, Ithaca, U.S.A.

J. Alexander, J. Chaves, J. Chu, S. Dittmer, K. Mcdermott, N. Mirman, G. Nicolas Kaufman, J.R. Patterson, A. Rinkevicius, A. Ryd, L. Skinnari, L. Soffi, S.M. Tan, Z. Tao, J. Thom, J. Tucker, P. Wittich, M. Zientek

Fairfield University, Fairfield, U.S.A.

D. Winn

Fermi National Accelerator Laboratory, Batavia, U.S.A.

S. Abdullin, M. Albrow, G. Apollinari, A. Apresyan, S. Banerjee, L.A.T. Bauerdick, A. Beretvas, J. Berryhill, P.C. Bhat, G. Bolla, K. Burkett, J.N. Butler, H.W.K. Cheung, F. Chlebana, S. Cihangir†, M. Cremonesi, V.D. Elvira, I. Fisk, J. Freeman, E. Gottschalk, L. Gray, D. Green, S. Grünendahl, O. Gutsche, D. Hare, R.M. Harris, S. Hasegawa, J. Hirschauer, Z. Hu, B. Jayatilaka, S. Jindariani, M. Johnson, U. Joshi, B. Klima, B. Kreis, S. Lammel, J. Linacre, D. Lincoln, R. Lipton, T. Liu, R. Lopes De Sá, J. Lykken, K. Maeshima, N. Magini, J.M. Marraffino, S. Maruyama, D. Mason, P. McBride, P. Merkel, S. Mrenna, S. Nahn, V. O'Dell, K. Pedro, O. Prokofyev, G. Rakness, L. Ristori, E. Sexton-Kennedy, A. Soha, W.J. Spalding, L. Spiegel, S. Stoynev, N. Strobbe, L. Taylor, S. Tkaczyk, N.V. Tran, L. Uplegger, E.W. Vaandering, C. Vernieri, M. Verzocchi, R. Vidal, M. Wang, H.A. Weber, A. Whitbeck, Y. Wu

University of Florida, Gainesville, U.S.A.

D. Acosta, P. Avery, P. Bortignon, D. Bourilkov, A. Brinkerhoff, A. Carnes, M. Carver, D. Curry, S. Das, R.D. Field, I.K. Furic, J. Konigsberg, A. Korytov, J.F. Low, P. Ma, K. Matchev, H. Mei, G. Mitselmakher, D. Rank, L. Shchutska, D. Sperka, L. Thomas, J. Wang, S. Wang, J. Yelton

Florida International University, Miami, U.S.A.

S. Linn, P. Markowitz, G. Martinez, J.L. Rodriguez

Florida State University, Tallahassee, U.S.A.

A. Ackert, T. Adams, A. Askew, S. Bein, S. Hagopian, V. Hagopian, K.F. Johnson, H. Prosper, A. Santra, R. Yohay

Florida Institute of Technology, Melbourne, U.S.A.

M.M. Baarmand, V. Bhopatkar, S. Colafranceschi, M. Hohlmann, D. Noonan, T. Roy, F. Yumiceva

University of Illinois at Chicago (UIC), Chicago, U.S.A.

M.R. Adams, L. Apanasevich, D. Berry, R.R. Betts, I. Bucinskaite, R. Cavanaugh, O. Evdokimov, L. Gauthier, C.E. Gerber, D.J. Hofman, K. Jung, I.D. Sandoval Gonzalez, N. Varelas, H. Wang, Z. Wu, M. Zakaria, J. Zhang

The University of Iowa, Iowa City, U.S.A.

B. Bilki[68], W. Clarida, K. Dilsiz, S. Durgut, R.P. Gandrajula, M. Haytmyradov, V. Khristenko, J.-P. Merlo, H. Mermerkaya[69], A. Mestvirishvili, A. Moeller, J. Nachtman, H. Ogul, Y. Onel, F. Ozok[70], A. Penzo, C. Snyder, E. Tiras, J. Wetzel, K. Yi

Johns Hopkins University, Baltimore, U.S.A.

I. Anderson, B. Blumenfeld, A. Cocoros, N. Eminizer, D. Fehling, L. Feng, A.V. Gritsan, P. Maksimovic, C. Martin, M. Osherson, J. Roskes, U. Sarica, M. Swartz, M. Xiao, Y. Xin, C. You

The University of Kansas, Lawrence, U.S.A.

A. Al-bataineh, P. Baringer, A. Bean, S. Boren, J. Bowen, J. Castle, L. Forthomme, R.P. Kenny III, S. Khalil, A. Kropivnitskaya, D. Majumder, W. Mcbrayer, M. Murray, S. Sanders, R. Stringer, J.D. Tapia Takaki, Q. Wang

Kansas State University, Manhattan, U.S.A.

A. Ivanov, K. Kaadze, Y. Maravin, A. Mohammadi, L.K. Saini, N. Skhirtladze, S. Toda

Lawrence Livermore National Laboratory, Livermore, U.S.A.

F. Rebassoo, D. Wright

University of Maryland, College Park, U.S.A.

C. Anelli, A. Baden, O. Baron, A. Belloni, B. Calvert, S.C. Eno, C. Ferraioli, J.A. Gomez, N.J. Hadley, S. Jabeen, R.G. Kellogg, T. Kolberg, J. Kunkle, Y. Lu, A.C. Mignerey, F. Ricci-Tam, Y.H. Shin, A. Skuja, M.B. Tonjes, S.C. Tonwar

Massachusetts Institute of Technology, Cambridge, U.S.A.

D. Abercrombie, B. Allen, A. Apyan, V. Azzolini, R. Barbieri, A. Baty, R. Bi, K. Bierwagen, S. Brandt, W. Busza, I.A. Cali, M. D'Alfonso, Z. Demiragli, L. Di Matteo, G. Gomez Ceballos, M. Goncharov, D. Hsu, Y. Iiyama, G.M. Innocenti, M. Klute, D. Kovalskyi, K. Krajczar, Y.S. Lai, Y.-J. Lee, A. Levin, P.D. Luckey, B. Maier, A.C. Marini, C. Mcginn, C. Mironov, S. Narayanan, X. Niu, C. Paus, C. Roland, G. Roland, J. Salfeld-Nebgen, G.S.F. Stephans, K. Tatar, M. Varma, D. Velicanu, J. Veverka, J. Wang, T.W. Wang, B. Wyslouch, M. Yang

University of Minnesota, Minneapolis, U.S.A.

A.C. Benvenuti, R.M. Chatterjee, A. Evans, P. Hansen, S. Kalafut, S.C. Kao, Y. Kubota, Z. Lesko, J. Mans, S. Nourbakhsh, N. Ruckstuhl, R. Rusack, N. Tambe, J. Turkewitz

University of Mississippi, Oxford, U.S.A.

J.G. Acosta, S. Oliveros

University of Nebraska-Lincoln, Lincoln, U.S.A.

E. Avdeeva, R. Bartek[71], K. Bloom, D.R. Claes, A. Dominguez[71], C. Fangmeier, R. Gonzalez Suarez, R. Kamalieddin, I. Kravchenko, A. Malta Rodrigues, F. Meier, J. Monroy, J.E. Siado, G.R. Snow, B. Stieger

State University of New York at Buffalo, Buffalo, U.S.A.

M. Alyari, J. Dolen, A. Godshalk, C. Harrington, I. Iashvili, J. Kaisen, A. Kharchilava, A. Parker, S. Rappoccio, B. Roozbahani

Northeastern University, Boston, U.S.A.

G. Alverson, E. Barberis, A. Hortiangtham, A. Massironi, D.M. Morse, D. Nash, T. Orimoto, R. Teixeira De Lima, D. Trocino, R.-J. Wang, D. Wood

Northwestern University, Evanston, U.S.A.

S. Bhattacharya, O. Charaf, K.A. Hahn, A. Kumar, N. Mucia, N. Odell, B. Pollack, M.H. Schmitt, K. Sung, M. Trovato, M. Velasco

University of Notre Dame, Notre Dame, U.S.A.

N. Dev, M. Hildreth, K. Hurtado Anampa, C. Jessop, D.J. Karmgard, N. Kellams, K. Lannon, N. Marinelli, F. Meng, C. Mueller, Y. Musienko[36], M. Planer, A. Reinsvold, R. Ruchti, G. Smith, S. Taroni, M. Wayne, M. Wolf, A. Woodard

The Ohio State University, Columbus, U.S.A.

J. Alimena, L. Antonelli, B. Bylsma, L.S. Durkin, S. Flowers, B. Francis, A. Hart, C. Hill, R. Hughes, W. Ji, B. Liu, W. Luo, D. Puigh, B.L. Winer, H.W. Wulsin

Princeton University, Princeton, U.S.A.

S. Cooperstein, O. Driga, P. Elmer, J. Hardenbrook, P. Hebda, D. Lange, J. Luo, D. Marlow, T. Medvedeva, K. Mei, J. Olsen, C. Palmer, P. Piroué, D. Stickland, A. Svyatkovskiy, C. Tully

University of Puerto Rico, Mayaguez, U.S.A.

S. Malik

Purdue University, West Lafayette, U.S.A.

A. Barker, V.E. Barnes, S. Folgueras, L. Gutay, M.K. Jha, M. Jones, A.W. Jung, A. Khatiwada, D.H. Miller, N. Neumeister, J.F. Schulte, X. Shi, J. Sun, F. Wang, W. Xie

Purdue University Calumet, Hammond, U.S.A.

N. Parashar, J. Stupak

Rice University, Houston, U.S.A.

A. Adair, B. Akgun, Z. Chen, K.M. Ecklund, F.J.M. Geurts, M. Guilbaud, W. Li, B. Michlin, M. Northup, B.P. Padley, J. Roberts, J. Rorie, Z. Tu, J. Zabel

University of Rochester, Rochester, U.S.A.

B. Betchart, A. Bodek, P. de Barbaro, R. Demina, Y.t. Duh, T. Ferbel, M. Galanti, A. Garcia-Bellido, J. Han, O. Hindrichs, A. Khukhunaishvili, K.H. Lo, P. Tan, M. Verzetti

Rutgers, The State University of New Jersey, Piscataway, U.S.A.

A. Agapitos, J.P. Chou, Y. Gershtein, T.A. Gómez Espinosa, E. Halkiadakis, M. Heindl, E. Hughes, S. Kaplan, R. Kunnawalkam Elayavalli, S. Kyriacou, A. Lath, K. Nash, H. Saka, S. Salur, S. Schnetzer, D. Sheffield, S. Somalwar, R. Stone, S. Thomas, P. Thomassen, M. Walker

University of Tennessee, Knoxville, U.S.A.

A.G. Delannoy, M. Foerster, J. Heideman, G. Riley, K. Rose, S. Spanier, K. Thapa

Texas A&M University, College Station, U.S.A.

O. Bouhali[72], A. Celik, M. Dalchenko, M. De Mattia, A. Delgado, S. Dildick, R. Eusebi, J. Gilmore, T. Huang, E. Juska, T. Kamon[73], R. Mueller, Y. Pakhotin, R. Patel, A. Perloff, L. Perniè, D. Rathjens, A. Safonov, A. Tatarinov, K.A. Ulmer

Texas Tech University, Lubbock, U.S.A.

N. Akchurin, C. Cowden, J. Damgov, F. De Guio, C. Dragoiu, P.R. Dudero, J. Faulkner, E. Gurpinar, S. Kunori, K. Lamichhane, S.W. Lee, T. Libeiro, T. Peltola, S. Undleeb, I. Volobouev, Z. Wang

Vanderbilt University, Nashville, U.S.A.

S. Greene, A. Gurrola, R. Janjam, W. Johns, C. Maguire, A. Melo, H. Ni, P. Sheldon, S. Tuo, J. Velkovska, Q. Xu

University of Virginia, Charlottesville, U.S.A.

M.W. Arenton, P. Barria, B. Cox, J. Goodell, R. Hirosky, A. Ledovskoy, H. Li, C. Neu, T. Sinthuprasith, X. Sun, Y. Wang, E. Wolfe, F. Xia

Wayne State University, Detroit, U.S.A.

C. Clarke, R. Harr, P.E. Karchin, J. Sturdy

University of Wisconsin - Madison, Madison, WI, U.S.A.

D.A. Belknap, J. Buchanan, C. Caillol, S. Dasu, L. Dodd, S. Duric, B. Gomber, M. Grothe, M. Herndon, A. Hervé, P. Klabbers, A. Lanaro, A. Levine, K. Long, R. Loveless, I. Ojalvo, T. Perry, G.A. Pierro, G. Polese, T. Ruggles, A. Savin, N. Smith, W.H. Smith, D. Taylor, N. Woods

†: Deceased
1: Also at Vienna University of Technology, Vienna, Austria
2: Also at State Key Laboratory of Nuclear Physics and Technology, Peking University, Beijing, China
3: Also at Institut Pluridisciplinaire Hubert Curien (IPHC), Université de Strasbourg, CNRS/IN2P3, Strasbourg, France
4: Also at Universidade Estadual de Campinas, Campinas, Brazil
5: Also at Universidade Federal de Pelotas, Pelotas, Brazil
6: Also at Université Libre de Bruxelles, Bruxelles, Belgium
7: Also at Deutsches Elektronen-Synchrotron, Hamburg, Germany
8: Also at Joint Institute for Nuclear Research, Dubna, Russia
9: Now at Cairo University, Cairo, Egypt
10: Also at Fayoum University, El-Fayoum, Egypt
11: Now at British University in Egypt, Cairo, Egypt
12: Now at Ain Shams University, Cairo, Egypt
13: Also at Université de Haute Alsace, Mulhouse, France
14: Also at Skobeltsyn Institute of Nuclear Physics, Lomonosov Moscow State University, Moscow, Russia

15: Also at Tbilisi State University, Tbilisi, Georgia

16: Also at CERN, European Organization for Nuclear Research, Geneva, Switzerland

17: Also at RWTH Aachen University, III. Physikalisches Institut A, Aachen, Germany

18: Also at University of Hamburg, Hamburg, Germany

19: Also at Brandenburg University of Technology, Cottbus, Germany

20: Also at Institute of Nuclear Research ATOMKI, Debrecen, Hungary

21: Also at MTA-ELTE Lendület CMS Particle and Nuclear Physics Group, Eötvös Loránd University, Budapest, Hungary

22: Also at Institute of Physics, University of Debrecen, Debrecen, Hungary

23: Also at Indian Institute of Science Education and Research, Bhopal, India

24: Also at Institute of Physics, Bhubaneswar, India

25: Also at University of Visva-Bharati, Santiniketan, India

26: Also at University of Ruhuna, Matara, Sri Lanka

27: Also at Isfahan University of Technology, Isfahan, Iran

28: Also at Yazd University, Yazd, Iran

29: Also at Plasma Physics Research Center, Science and Research Branch, Islamic Azad University, Tehran, Iran

30: Also at Università degli Studi di Siena, Siena, Italy

31: Also at Purdue University, West Lafayette, U.S.A.

32: Also at International Islamic University of Malaysia, Kuala Lumpur, Malaysia

33: Also at Malaysian Nuclear Agency, MOSTI, Kajang, Malaysia

34: Also at Consejo Nacional de Ciencia y Tecnología, Mexico city, Mexico

35: Also at Warsaw University of Technology, Institute of Electronic Systems, Warsaw, Poland

36: Also at Institute for Nuclear Research, Moscow, Russia

37: Now at National Research Nuclear University 'Moscow Engineering Physics Institute' (MEPhI), Moscow, Russia

38: Also at St. Petersburg State Polytechnical University, St. Petersburg, Russia

39: Also at University of Florida, Gainesville, U.S.A.

40: Also at P.N. Lebedev Physical Institute, Moscow, Russia

41: Also at California Institute of Technology, Pasadena, U.S.A.

42: Also at Budker Institute of Nuclear Physics, Novosibirsk, Russia

43: Also at Faculty of Physics, University of Belgrade, Belgrade, Serbia

44: Also at INFN Sezione di Roma; Università di Roma, Roma, Italy

45: Also at University of Belgrade, Faculty of Physics and Vinca Institute of Nuclear Sciences, Belgrade, Serbia

46: Also at Scuola Normale e Sezione dell'INFN, Pisa, Italy

47: Also at National and Kapodistrian University of Athens, Athens, Greece

48: Also at Riga Technical University, Riga, Latvia

49: Also at Institute for Theoretical and Experimental Physics, Moscow, Russia

50: Also at Albert Einstein Center for Fundamental Physics, Bern, Switzerland

51: Also at Istanbul Aydin University, Istanbul, Turkey

52: Also at Mersin University, Mersin, Turkey

53: Also at Cag University, Mersin, Turkey

54: Also at Piri Reis University, Istanbul, Turkey

55: Also at Gaziosmanpasa University, Tokat, Turkey

56: Also at Adiyaman University, Adiyaman, Turkey

57: Also at Ozyegin University, Istanbul, Turkey

58: Also at Izmir Institute of Technology, Izmir, Turkey

59: Also at Marmara University, Istanbul, Turkey
60: Also at Kafkas University, Kars, Turkey
61: Also at Istanbul Bilgi University, Istanbul, Turkey
62: Also at Yildiz Technical University, Istanbul, Turkey
63: Also at Hacettepe University, Ankara, Turkey
64: Also at Rutherford Appleton Laboratory, Didcot, U.K.
65: Also at School of Physics and Astronomy, University of Southampton, Southampton, U.K.
66: Also at Instituto de Astrofísica de Canarias, La Laguna, Spain
67: Also at Utah Valley University, Orem, U.S.A.
68: Also at Argonne National Laboratory, Argonne, U.S.A.
69: Also at Erzincan University, Erzincan, Turkey
70: Also at Mimar Sinan University, Istanbul, Istanbul, Turkey
71: Now at The Catholic University of America, Washington, U.S.A.
72: Also at Texas A&M University at Qatar, Doha, Qatar
73: Also at Kyungpook National University, Daegu, Korea